Warm-fluid description of intense beam equilibrium and electrostatic stability properties

Steven M. Lund
University of California, Lawrence Livermore National Laboratory, Livermore, California 94550

Ronald C. Davidson
Plasma Physics Laboratory, Princeton University, Princeton, New Jersey 08543

(Received 30 March 1998; accepted 16 April 1998)

A nonrelativistic warm-fluid model is employed in the electrostatic approximation to investigate the equilibrium and stability properties of an unbunched, continuously focused intense ion beam. A closed macroscopic model is obtained by truncating the hierarchy of moment equations by the assumption of negligible heat flow. Equations describing self-consistent fluid equilibria are derived and elucidated with examples corresponding to thermal equilibrium, the Kapchinskij–Vladimirskij (KV) equilibrium, and the waterbag equilibrium. Linearized fluid equations are derived that describe the evolution of small-amplitude perturbations about an arbitrary equilibrium. Electrostatic stability properties are analyzed in detail for a cold beam with step-function density profile, and then for axisymmetric flute perturbations with $\partial/\partial\theta=0$ and $\partial/\partial z=0$ about a warm-fluid KV beam equilibrium. The radial eigenfunction describing axisymmetric flute perturbations about the KV equilibrium is found to be *identical* to the eigenfunction derived in a full kinetic treatment. However, in contrast to the kinetic treatment, the warm-fluid model predicts stable oscillations. None of the instabilities that are present in a kinetic description are obtained in the fluid model. A careful comparison of the mode oscillation frequencies associated with the fluid and kinetic models is made in order to delineate which stability features of a KV beam are model-dependent and which may have general applicability. [S1070-664X(98)00508-4]

I. INTRODUCTION

In recent years, there has been increasing interest in the equilibrium and stability properties of intense ion beams.[1–4] Potential applications include heavy-ion-driven production of inertial fusion energy, transmutation of radioactive waste, spallation neutron sources, and accelerator-based production of tritium.[5–9] Such intense beam applications necessitate the study of beam transport in a regime where space-charge effects and collective oscillations are important.[10–32] Recent experiments and simulation studies suggest that such modes can play a deleterious role in intense beam transport.[33–44] In general, an analysis of collective modes in intense nonneutral beams requires knowledge of the beam distribution function in six-dimensional phase space in order to carry out numerical simulations using the distribution function as an initial condition, or to perform analytical studies of equilibrium and stability properties using kinetic theory. Although analytical studies provide valuable insight regarding parametric behavior, such kinetic analyses can become quite complex, even under highly idealized assumptions.[10–32] Further complicating this situation is the fact that the detailed form of the initial distribution function entering the accelerator is often unknown due to various nonideal effects in the region near the beam source. Moreover, for the case of periodic focusing channels, the transverse Kapchinskij–Vladimirskij (KV) distribution[10] is the only distribution function for which the kinetic equilibrium and linear stability properties have been determined analytically.[10–21]

Unfortunately, the KV distribution, which forms much of the basis for present analytical understanding of the collective stability properties of intense beams, also has an unphysical, highly inverted phase-space population. This inverted population provides the free energy to drive progressively more modes of oscillation unstable with increasing space-charge strength.[1,11–20] Many of these instabilities are regarded as unphysical, since they are not observed in particle-in-cell simulations of more realistic initial distributions with noninverted, monotonic decreasing phase-space populations.[33] Furthermore, the KV distribution tends to overestimate the effects of instabilities because all particles in the equilibrium distribution have the same frequency of transverse particle oscillation (i.e., the depressed betatron frequency ν) rather than a more realistic spread of oscillation frequencies. Thus, the entire KV equilibrium distribution participates in any instability rather than only a portion of the distribution as would be anticipated in a more realistic model.

Because of these pathologies, many aspects of the kinetic modes associated with the KV distribution are commonly regarded as being of limited practical value. Nevertheless, the two-dimensional transverse phase-space projections of a KV beam are not too dissimilar from those observed in intense beam experiments and in simulations with more realistic initial distributions. Furthermore, the collective modes observed in experiment and simulation can be similar in structure to those studied analytically using the KV distribution. For example, the simplest linear kinetic mode supported by the KV model is the so-called ''envelope''

mode[45,1,2] which is characterized by a uniform density perturbation in each transverse beam slice, and a related change in the envelope radius. This envelope mode is experimentally observed and has a well-known parametric instability in periodic focusing channels when the phase advance per focusing period of the envelope of beam particles becomes too large. Other kinetic modes supported by the KV distribution have more detailed transverse structures[11–19] that are suggestive of classes of perturbations observed experimentally,[40–43] but typically exhibit instabilities that are inconsistent with experimental evidence. Thus, certain features of the KV model appear to be relevant to realistic beams, while others do not. The purpose of this paper is to better understand how the collective modes associated with the KV distribution change under different model assumptions, so as to learn which features are model-dependent and which are likely to have general applicability. Such knowledge should prove valuable because the KV distribution provides considerable analytical insight into the mode structure. In turn, these simplified models can then provide valuable guidance regarding possible structure resonances and other destabilizing effects of practical importance.

The standard kinetic description of an intense beam is based on the nonlinear Vlasov–Maxwell equations, where the beam is regarded as a collisionless non-neutral plasma.[46] Vlasov stability analyses are generally difficult due to the need to evaluate orbit integrals that describe how small-amplitude perturbations evolve by integrating along the particle trajectories in the equilibrium field configuration. In contrast, a macroscopic fluid model[47,48] offers the prospect for a more straightforward stability analysis. The simplicity of a fluid description results from the fact that the beam is described in terms of local macroscopic variables obtained by averaging over the momentum-space dependence of the kinetic distribution function. Furthermore, a fluid model can lead to results that are more amenable to physical interpretation, because the fluid variables consist of readily understood macroscopic quantities. As a general remark, while macroscopic fluid models[47–54] have been applied to a number of intense beam problems ranging from studies of the electromagnetic filamentation instability,[51,52] to intense equilibrium flow in uniform[53] and periodic[54] focusing systems, there are few instances[49,50] where thermal effects are included in a self-consistent manner.

In this paper, we employ a warm-fluid model to analyze the equilibrium and electrostatic stability properties of an unbunched, intense ion beam propagating in the absence of acceleration. Equations are derived describing self-consistent fluid equilibria and the evolution of small-amplitude perturbations about an arbitrary equilibrium. For simplicity, the analysis is carried out in the nonrelativistic, electrostatic regime, and a continuous, applied focusing field is assumed, corresponding to either a solenoidal magnetic field and/or a radial electric field produced by a fixed uniform charge background. The macroscopic fluid model is based on the hierarchy of moments of the Vlasov equation, truncated by assuming negligible heat flow, which yields a closed system of equations.[47] Such a model incorporates average thermal effects through an anisotropic pressure tensor, which evolves self-consistently in the absence of heat flow. This contrasts with the simpler cold-fluid approximation, where thermal effects are neglected under the assumption of negligible fluid pressure. The fluid model employed in the present analysis is expected to be valid for high-frequency collective modes. Low-frequency modes which may be influenced by heat flow are beyond the scope of the truncation model.

The fluid equations are employed to derive eigenvalue equations that describe general perturbations about arbitrary cold-beam equilibria, and axisymmetric flute perturbations with $\partial/\partial\theta = 0$ and $\partial/\partial z = 0$ about arbitrary warm-beam equilibria. The cold-fluid eigenvalue equation is analyzed to determine the stability properties of a step-function equilibrium density profile, which is equivalent to a cold KV beam. The warm-fluid eigenvalue equation is analytically solved for a warm KV beam equilibrium to determine the transverse fluid stability properties of a KV beam. Results are compared to those previously obtained in the kinetic treatment by Gluckstern.[11] These comparisons help to elucidate which features of the kinetic model are a consequence of the detailed phase-space structure of the KV distribution function, and which features are a consequence of the bulk (macroscopic) properties of the distribution. Since the detailed phase-space dependence of the KV distribution is somewhat pathological, whereas the macroscopic properties are similar to those of more realistic beams, this comparison helps to delineate which features of the kinetic KV model are likely to be of practical importance.

This paper is organized as follows. First, in Sec. II, a closed fluid model is derived for a propagating intense beam by truncating the hierarchy of moments of the Vlasov equation under the assumption of negligible heat flow and a diagonal pressure tensor. The basic equations for the warm-fluid model, describing both the equilibrium properties and the evolution of small-amplitude perturbations about an arbitrary equilibrium, are presented in Sec. III. The equilibrium fluid equations (Sec. III A) are elucidated with examples corresponding to thermal equilibrium, the KV equilibrium, and the waterbag equilibrium, which are familiar examples from the kinetic theory of a continuously focused beam.[1,2] Following a derivation of the linearized equations describing the evolution of small-amplitude perturbations about an arbitrary fluid equilibrium (Sec. III B), simplified eigenvalue equations are derived in the cold-beam limit (Sec. III C), and for the case of axisymmetric flute perturbations with $\partial/\partial\theta = 0$ and $\partial/\partial z = 0$ in the warm-beam case (Sec. III D). These simplified eigenvalue equations are employed to analyze the macroscopic stability properties of a KV beam equilibrium in Secs. IV and V. First, for reference, the eigenfunction and normal modes describing perturbations about a cold KV beam equilibrium with a step-function density profile are reviewed in Sec. IV. Particular attention is given to a bifurcation of the eigenfunction as the total canonical angular momentum of the cold-beam equilibrium changes from zero to a nonzero value. Second, the radial eigenfunction and normal modes describing axisymmetric flute perturbations with $\partial/\partial\theta = 0$ and $\partial/\partial z = 0$ are analyzed for the warm-beam case in Sec. V. This eigenfunction is found to be *identical* to the eigenfunction first derived by Gluckstern[11] using a kinetic

description. (These so-called Gluckstern kinetic modes are reviewed in Appendix B.) However, in contrast to the kinetic model, the dispersion relation is found to be simpler in the warm-fluid treatment, and it predicts a single, stable mode of oscillation, rather than the discrete spectrum of (possibly unstable) oscillation frequencies obtained in the kinetic treatment. It is found that the single oscillation frequency obtained from the fluid dispersion relation is a good approximation to the highest-frequency branch of the kinetic dispersion relation—which is always stable. This close correspondence is shown to be exact in the limits of vanishing and maximum (focusing limit) space-charge strengths. Together, these results are used to argue that the highest-frequency branch of the kinetic dispersion relation is fluid-like, and consequently is associated with the bulk (macroscopic) features of the KV equilibrium rather than the detailed phase-space structure—suggestive of general applicability.

II. THEORETICAL MODEL AND ASSUMPTIONS

In the present analysis, we consider a single-species, intense non-neutral beam of charged particles with characteristic beam radius r_b and axial velocity $V_z \simeq V_b = \text{const}$ propagating in the z direction parallel to a uniform focusing solenoidal magnetic field

$$\mathbf{B}^{\text{sol}}(\mathbf{x}) = B_f \hat{\mathbf{e}}_z, \tag{1}$$

where $B_f = \text{const}$. To model an additional radial-focusing force, we assume a (fictitious) fixed, uniform charge background which produces an effective radial electric field $\mathbf{E}^f(\mathbf{x})$ defined by

$$\mathbf{E}^f(\mathbf{x}) = -\frac{m}{Z_i e}\,\omega_f^2 (x\hat{\mathbf{e}}_x + y\hat{\mathbf{e}}_y) \tag{2}$$

over the radial extent of the beam. Here, $Z_i e$ and m are the charge and rest mass, respectively, of a beam particle, $\omega_f^2 = \text{const}$ has the dimensions of frequency-squared, and the transverse coordinates (x,y) are measured from the beam axis at $x=0=y$. The focusing electric field in Eq. (2) would be produced by a uniformly distributed background with charge density $\rho_f = -m\omega_f^2/2\pi Z_i e = \text{const}$. Such a uniform charge background is often used to model the *average* focusing properties of an alternating-gradient lattice of electric or magnetic quadrupoles.[1,2] For future reference, we introduce simplified terminology for two important special focusing field configurations, and refer to the case where $\omega_f \neq 0$ and $B_f = 0$ as *pure electric* focusing, and the case where $B_f \neq 0$ and $\omega_f = 0$ as *pure magnetic* focusing. In addition, the space charge and current of the charged particles composing the beam generally produce self-electric and self-magnetic fields, $\mathbf{E}^s(\mathbf{x},t)$ and $\mathbf{B}^s(\mathbf{x},t)$, which can be expressed as $\mathbf{E}^s = -\nabla\phi - (1/c)\partial\mathbf{A}/\partial t$, and $\mathbf{B}^s = \nabla\times\mathbf{A}$. For simplicity, the present analysis treats the dynamics of the beam particles *nonrelativistically*, and the self-magnetic field generated by the average beam current is neglected. In addition, field perturbations with *transverse electromagnetic* polarization are neglected, and self-field effects are treated in the electrostatic approximation with $\mathbf{B}^s \simeq 0$ and

$$\mathbf{E}^s(\mathbf{x},t) = -\nabla\phi(\mathbf{x},t), \tag{3}$$

where $\phi(\mathbf{x},t)$ is the electrostatic self-field potential. The beam particles of course interact with the total electric and magnetic fields, $\mathbf{E}^f + \mathbf{E}^s$ and $\mathbf{B}^{\text{sol}}$, causing a corresponding change in the beam distribution function $f(\mathbf{x},\mathbf{p},t)$ as it evolves in the phase space $(\mathbf{x},\mathbf{p})$.

Consistent with the assumption of a nonrelativistic beam with $\beta_b = V_b/c \ll 1$ and the neglect of magnetic self-fields,[1] it assumed that Budker's parameter ν satisfies

$$\nu = \frac{Z_i^2 e^2 N}{mc^2} \ll 1. \tag{4}$$

Here, c is the speed of light *in vacuo*, $N = \int dx\,dy\; n$ is the number of beam particles per unit axial length, and $n(\mathbf{x},t) = \int d^3p\; f(\mathbf{x},\mathbf{p},t)$ is the number density of beam particles. While the inequality in Eq. (4) assures that the self-fields are sufficiently weak in absolute intensity that the characteristic potential energy $Z_i e\phi$ satisfies $|Z_i e\phi/mc^2| \ll 1$, the present analysis does permit $Z_i e\phi$ to be comparable in size with the transverse kinetic energy $(p_x^2 + p_y^2)/2m$ of a beam particle.

For the field configuration in Eqs. (1)–(3), the distribution function $f(\mathbf{x},\mathbf{p},t)$ of the beam particles evolves according to the nonlinear Vlasov equation[46]

$$\left\{\frac{\partial}{\partial t} + \mathbf{v}\cdot\frac{\partial}{\partial\mathbf{x}} + Z_i e\left[-\nabla\phi + \mathbf{E}^f + \frac{1}{c}\,\mathbf{v}\times B_f\hat{\mathbf{e}}_z\right]\cdot\frac{\partial}{\partial\mathbf{p}}\right\} f = 0. \tag{5}$$

Here, $\mathbf{v} = \mathbf{p}/m$ is the (nonrelativistic) velocity, $\mathbf{E}^f(\mathbf{x}) = -(m\omega_f^2/Z_i e)\mathbf{x}_\perp$ is the focusing electric field due to the ''fixed'' background charge, and $\phi(\mathbf{x},t)$ is determined self-consistently in terms of the distribution function $f(\mathbf{x},\mathbf{p},t)$ from Poisson's equation

$$\nabla^2\phi = -4\pi Z_i e n = -4\pi Z_i e \int d^3p\; f. \tag{6}$$

For present purposes, a perfectly conducting cylindrical wall is assumed to be located at radius $r = r_w = \text{const}$. Imposing the requirement that the tangential electric field is equal to zero at $r = r_w$, i.e., $[\partial\phi/\partial z]_{r=r_w} = 0 = [r^{-1}\partial\phi/\partial\theta]_{r=r_w}$, then gives the boundary condition

$$\phi(r = r_w, \theta, z, t) = \text{const} \tag{7}$$

for the self-field potential. Here, (r,θ,z) are cylindrical polar coordinates, where $x = r\cos\theta$ and $y = r\sin\theta$, and $r = (x^2 + y^2)^{1/2}$ is the radial distance from the beam axis. Equations (5) and (6) can be used to investigate the nonlinear beam dynamics, collective processes, and linear stability properties over a wide range of system parameters consistent with the assumptions enumerated earlier in this section. For present purposes, however, we make use of Eq. (5) to derive a set of macroscopic fluid equations that describe the self-consistent evolution of the system.

As is customary in a *macroscopic fluid description* of charged particle systems, we introduce the fluid quantities corresponding to particle density $n(\mathbf{x},t)$, average flow velocity $\mathbf{V}(\mathbf{x},t)$, pressure tensor $\mathbf{P}(\mathbf{x},t)$, and heat flow tensor $\mathbf{Q}(\mathbf{x},t)$ defined in terms of the distribution function $f(\mathbf{x},\mathbf{p},t)$ by[47]

$$n=\int d^3p\ f,$$

$$n\mathbf{V}=\int d^3p\ \mathbf{v}f,$$

$$\mathbf{P}=\int d^3p(\mathbf{v}-\mathbf{V})(\mathbf{p}-m\mathbf{V})f, \tag{8}$$

$$\mathbf{Q}=\int d^3p(\mathbf{v}-\mathbf{V})(\mathbf{v}-\mathbf{V})(\mathbf{p}-m\mathbf{V})f,$$

$$\vdots$$

Operating on Eq. (5) with $\int d^3p\cdots$ and taking successive momentum moments as indicated by Eq. (8) leads to the chain of macroscopic moment equations advancing n, $\mathbf{V}$, $\mathbf{P}$,..., i.e.,

$$\frac{\partial}{\partial t}n+\frac{\partial}{\partial \mathbf{x}}\cdot(n\mathbf{V})=0, \tag{9}$$

$$mn\left(\frac{\partial}{\partial t}+\mathbf{V}\cdot\frac{\partial}{\partial \mathbf{x}}\right)\mathbf{V}+\frac{\partial}{\partial \mathbf{x}}\cdot\mathbf{P}$$
$$=Z_ien\left(-\frac{\partial\phi}{\partial \mathbf{x}}+\mathbf{E}^f+\frac{1}{c}\mathbf{V}\times B_f\hat{\mathbf{e}}_z\right), \tag{10}$$

$$\frac{\partial}{\partial t}\mathbf{P}+\frac{\partial}{\partial \mathbf{x}}\cdot(\mathbf{VP})+\mathbf{P}\cdot\left(\frac{\partial}{\partial \mathbf{x}}\mathbf{V}\right)+\left(\frac{\partial}{\partial \mathbf{x}}\mathbf{V}\right)^T\cdot\mathbf{P}+\frac{\partial}{\partial \mathbf{x}}\cdot\mathbf{Q}$$
$$=\frac{Z_ieB_f}{mc}(\mathbf{P}\times\hat{\mathbf{e}}_z-\hat{\mathbf{e}}_z\times\mathbf{P}),$$
$$\vdots \tag{11}$$

where $(\cdots)^T$ denotes dyadic transpose. Note from Eqs. (9) to (11), that lower-order moments are coupled, successively, to higher-order moments, e.g., the evolution of the beam density $n(\mathbf{x},t)$ is coupled to the flow velocity $\mathbf{V}(\mathbf{x},t)$ by the continuity equation (9), the evolution of $\mathbf{V}(\mathbf{x},t)$ is coupled to the pressure tensor $\mathbf{P}(\mathbf{x},t)$ by the force balance equation (10), and so on.

The simplest level of closure of the macroscopic moment equations (8)–(11) corresponds to the *cold-fluid approximation in* which the pressure-tensor contribution in Eq. (10) is neglected in comparison with other terms in the force-balance equation.[47] In this case, we approximate $(\partial/\partial\mathbf{x})\cdot\mathbf{P}\simeq 0$ in Eq. (10) and neglect the information in Eq. (11) and higher-order moment equations. While several aspects of equilibrium and stability properties can be investigated in such a cold-fluid model, many important effects associated with finite beam temperature and thermal anisotropy are necessarily absent. Therefore, in the present analysis, we retain finite-pressure effects and adopt a closure model in which the heat-flow contributions are treated as negligibly small in Eq. (11).[47] In this case, we approximate $(\partial/\partial\mathbf{x})\cdot\mathbf{Q}\simeq 0$ in Eq. (11), and the evolution of the pressure tensor $\mathbf{P}(\mathbf{x},t)$ is described by

$$\frac{\partial}{\partial t}\mathbf{P}+\frac{\partial}{\partial \mathbf{x}}\cdot(\mathbf{VP})+\mathbf{P}\cdot\left(\frac{\partial}{\partial \mathbf{x}}\mathbf{V}\right)+\left(\frac{\partial}{\partial \mathbf{x}}\mathbf{V}\right)^T\cdot\mathbf{P}$$
$$=\frac{Z_ieB_f}{mc}(\mathbf{P}\times\hat{\mathbf{e}}_z-\hat{\mathbf{e}}_z\times\mathbf{P}). \tag{12}$$

Equations (9), (10), and (12), when supplemented by Poisson's equation (6) and the appropriate boundary conditions, then constitute a closed system of equations that describe the self-consistent evolution of the beam density $n(\mathbf{x},t)$, flow velocity $\mathbf{V}(\mathbf{x},t)$, pressure tensor $\mathbf{P}(\mathbf{x},t)$, and electrostatic potential $\phi(\mathbf{x},t)$. This model should retain leading-order thermal effects that are describable in an average sense in terms of a macroscopic pressure. A model that assumes a diagonal form of the pressure tensor and $\partial/\partial z=0$ was first employed by Hofmann[49] to analyze beam stability properties.

Formally, the assumption of negligible heat flow $[(\partial/\partial\mathbf{x})\cdot\mathbf{Q}\simeq 0]$ in Eq. (11) is strictly justified when the particle distribution function f is an even function of v_j-V_j, where j denotes the x, y, or z Cartesian component of $\mathbf{v}$, etc. For an intense beam propagating near the space-charge limit of the applied focusing field, certain classes of transverse electrostatic oscillations (with time dependence $\propto e^{-i\omega t}$) are known from kinetic theory[10–19] to have frequencies of order the beam plasma frequency (i.e., $\omega\sim\omega_p$). In this situation, transverse single-particle oscillations ($\propto e^{-i\nu t}$) will be on a much slower time scale than these collective modes (i.e., $\omega\sim\omega_p\gg\nu$), because the defocusing space-charge field nearly cancels the applied focusing field. The influence of heat flow on modes with such rapid characteristic time scales should be small. On the other hand, approximations inherent in the present fluid model are likely to become more problematic for low-frequency collective modes (i.e., when $\omega\ll\omega_p$).

Equation (12) can be further simplified in the strong-focusing approximation, in which case the terms on the right-hand side of Eq. (12) (which are proportional to B_f) are treated as individually large in magnitude in comparison with the terms on the left-hand side of Eq. (12). We then conclude, in lowest order, that the pressure tensor $\mathbf{P}(\mathbf{x},t)$ necessarily satisfies

$$\mathbf{P}(\mathbf{x},t)\times\hat{\mathbf{e}}_z=\hat{\mathbf{e}}_z\times\mathbf{P}(\mathbf{x},t), \tag{13}$$

in which case $P(\mathbf{x},t)$ has the *diagonal* form

$$\mathbf{P}(\mathbf{x},t)=P_\perp(\mathbf{x},t)(\hat{\mathbf{e}}_x\hat{\mathbf{e}}_x+\hat{\mathbf{e}}_y\hat{\mathbf{e}}_y)+P_\parallel(\mathbf{x},t)\hat{\mathbf{e}}_z\hat{\mathbf{e}}_z. \tag{14}$$

Substituting Eq. (14) into Eq. (12), some straightforward algebra shows that the *perpendicular pressure* $P_\perp(\mathbf{x},t)$ and the *parallel pressure* $P_\parallel(\mathbf{x},t)$ evolve according to

$$\left(\frac{\partial}{\partial t}+\mathbf{V}\cdot\frac{\partial}{\partial \mathbf{x}}\right)P_\perp+2P_\perp\frac{\partial}{\partial \mathbf{x}}\cdot\mathbf{V}-P_\perp\frac{\partial V_z}{\partial z}=0, \tag{15}$$

and

$$\left(\frac{\partial}{\partial t}+\mathbf{V}\cdot\frac{\partial}{\partial \mathbf{x}}\right)P_\parallel+P_\parallel\frac{\partial}{\partial \mathbf{x}}\cdot\mathbf{V}+2P_\parallel\frac{\partial V_z}{\partial z}=0. \tag{16}$$

Here, $V_z(\mathbf{x},t)=\hat{\mathbf{e}}_z\cdot\mathbf{V}(\mathbf{x},t)$ is the axial component of flow velocity. In the subsequent analysis, we make use of Eqs. (6), (9), (10), (15) and (16) to provide a closed system of equations that describes the self-consistent evolution of the elec-

trostatic potential $\phi(\mathbf{x},t)$, density $n(\mathbf{x},t)$, flow velocity $\mathbf{V}(\mathbf{x},t)$, perpendicular pressure $P_\perp(\mathbf{x},t)$, and parallel pressure $P_\parallel(\mathbf{x},t)$. Making use of the continuity equation (9) to eliminate $(\partial/\partial\mathbf{x})\cdot\mathbf{V}$ in Eqs. (15) and (16), it is readily shown that Eqs. (15) and (16) can be expressed in the equivalent forms,

$$\left(\frac{\partial}{\partial t}+\mathbf{V}\cdot\frac{\partial}{\partial\mathbf{x}}\right)\left(\frac{P_\perp}{n^2}\right)-\frac{\partial V_z}{\partial z}\left(\frac{P_\perp}{n^2}\right)=0, \tag{17}$$

and

$$\left(\frac{\partial}{\partial t}+\mathbf{V}\cdot\frac{\partial}{\partial\mathbf{x}}\right)\left(\frac{P_\parallel}{n}\right)+2\frac{\partial V_z}{\partial z}\left(\frac{P_\parallel}{n}\right)=0. \tag{18}$$

Whenever $\partial/\partial z=0$, we note from Eqs. (17) and (18) that $P_\perp/n^2$ and $P_\parallel/n$ are constant following the (nonlinear) motion of a fluid element. Evidently, the role of the strong focusing field [Eqs. (13) and (14)] has an isotropizing effect similar to that of collisions. Note from Eq. (17) that when $\partial/\partial z=0$ the dependence of $P_\perp$ on n is *double adiabatic* ($P_\perp\propto n^2$), corresponding to *two* degrees of freedom in the plane perpendicular to $B_f\hat{\mathbf{e}}_z$. Hofmann showed that such a double-adiabatic equation of state is also valid in periodic focusing systems,[49] and for reasonable equilibria with $\mathbf{V}_\perp(r=0)=0$, it follows that $P_\perp/n^2|_{r=0}=\text{const}$. This constraint can be regarded as a generalization of beam emittance conservation for a periodically focused KV beam equilibrium to the case of periodically focused non-KV distributions.

The equilibrium and stability analysis in Secs. III–V is carried out in cylindrical polar coordinates (r,θ,z), where $x=r\cos\theta$, $y=r\sin\theta$, and $r=(x^2+y^2)^{1/2}$ is the radial distance from the beam axis. For completeness, we record here the complete set of dynamical equations for the beam density $n(r,\theta,z,t)$, flow velocity $\mathbf{V}=V_r(r,\theta,z,t)\hat{\mathbf{e}}_r+V_\theta(r,\theta,z,t)\hat{\mathbf{e}}_\theta+V_z(r,\theta,z,t)\hat{\mathbf{e}}_z$, and perpendicular and parallel pressures, $P_\perp(r,\theta,z,t)$ and $P_\parallel(r,\theta,z,t)$. In cylindrical coordinates, Eqs. (9), (10), (15), and (16) become

$$\frac{\partial}{\partial t}n+\frac{1}{r}\frac{\partial}{\partial r}(rnV_r)+\frac{1}{r}\frac{\partial}{\partial\theta}(nV_\theta)+\frac{\partial}{\partial z}(nV_z)=0, \tag{19}$$

$$mn\left(\frac{\partial}{\partial t}+V_r\frac{\partial}{\partial r}+\frac{V_\theta}{r}\frac{\partial}{\partial\theta}+V_z\frac{\partial}{\partial z}\right)V_r-n\frac{V_\theta^2}{r}+\frac{\partial}{\partial r}P_\perp$$
$$=Z_ien\left(-\frac{\partial}{\partial r}\phi-\frac{m\omega_f^2}{Z_ie}r+\frac{V_\theta}{c}B_f\right), \tag{20}$$

$$mn\left(\frac{\partial}{\partial t}+V_r\frac{\partial}{\partial r}+\frac{V_\theta}{r}\frac{\partial}{\partial\theta}+V_z\frac{\partial}{\partial z}\right)V_\theta+n\frac{V_\theta V_r}{r}+\frac{1}{r}\frac{\partial}{\partial\theta}P_\perp$$
$$=Z_ien\left(-\frac{1}{r}\frac{\partial}{\partial\theta}\phi-\frac{V_r}{c}B_f\right), \tag{21}$$

$$mn\left(\frac{\partial}{\partial t}+V_r\frac{\partial}{\partial r}+\frac{V_\theta}{r}\frac{\partial}{\partial\theta}+V_z\frac{\partial}{\partial z}\right)V_z+\frac{\partial}{\partial z}P_\parallel$$
$$=-Z_ien\frac{\partial}{\partial z}\phi, \tag{22}$$

$$\left(\frac{\partial}{\partial t}+V_r\frac{\partial}{\partial r}+\frac{V_\theta}{r}\frac{\partial}{\partial\theta}+V_z\frac{\partial}{\partial z}\right)P_\perp+2P_\perp\left(\frac{1}{r}\frac{\partial}{\partial r}rV_r+\frac{1}{r}\frac{\partial}{\partial\theta}V_\theta+\frac{\partial}{\partial z}V_z\right)-P_\perp\frac{\partial}{\partial z}V_z=0, \tag{23}$$

$$\left(\frac{\partial}{\partial t}+V_r\frac{\partial}{\partial r}+\frac{V_\theta}{r}\frac{\partial}{\partial\theta}+V_z\frac{\partial}{\partial z}\right)P_\parallel+P_\parallel\left(\frac{1}{r}\frac{\partial}{\partial r}rV_r+\frac{1}{r}\frac{\partial}{\partial\theta}V_\theta+\frac{\partial}{\partial z}V_z\right)+2P_\parallel\frac{\partial}{\partial z}V_z=0. \tag{24}$$

Equations (19)–(24) describe the nonlinear evolution of n, V_r, V_θ, V_z, $P_\perp$, and $P_\parallel$, and of course must be supplemented by Poisson's equation (6) for the electrostatic potential $\phi(r,\theta,z,t)$. In cylindrical coordinates, Eq. (6) can be expressed as

$$\left(\frac{1}{r}\frac{\partial}{\partial r}r\frac{\partial}{\partial r}+\frac{1}{r^2}\frac{\partial^2}{\partial\theta^2}+\frac{\partial^2}{\partial z^2}\right)\phi=-4\pi Z_ien. \tag{25}$$

In summary, Eqs. (19)–(25) together with the appropriate boundary and initial (time $t=0$) conditions constitute a closed macroscopic description of the nonlinear evolution of the system in the context of the present warm-fluid model. Most notably, Eqs. (19)–(25) incorporate the effects of pressure anisotropy, beam rotation, a focusing magnetic field $B_f\hat{\mathbf{e}}_z$, and a focusing electric field $\mathbf{E}^f=-(m/Z_ie)\omega_f^2r\hat{\mathbf{e}}_r$ due to a fixed, uniform charge background.

III. BASIC EQUATIONS

In this section we make use of Eqs. (19)–(25) to investigate equilibrium properties ($\partial/\partial t=0$) for axisymmetric beam propagation parallel to $B_f\hat{\mathbf{e}}_z$ (Sec. III A), and to derive linearized equations describing the evolution of small-amplitude perturbations (Sec. III B). The linearized equations are then used to obtain the electrostatic eigenvalue equation in the cold-beam approximation (Sec. III C). Finally, in the warm-beam case, the linearized equations are simplified for the special case of axisymmetric flute perturbations with $\partial/\partial\theta=0=\partial/\partial z$ (Sec. III D). Henceforth, all analysis is restricted to an unbunched beam equilibrium ($\partial/\partial z=0$) and, in practice, applies near the axial midpulse of a long-pulse beam.

A. Equilibrium properties

An *equilibrium analysis* of Eqs. (19)–(25) for axisymmetric, unbunched beam propagation proceeds by setting

$$\frac{\partial}{\partial t}=\frac{\partial}{\partial z}=\frac{\partial}{\partial\theta}=0, \tag{26}$$

corresponding to time-stationary solutions with no axial or azimuthal spatial variations. We denote the equilibrium profiles by $n^0(r)$, $V_r^0(r)$, $V_\theta^0(r)$, $V_z^0(r)$, $P_\perp^0(r)$, $P_\parallel^0(r)$, and $\phi^0(r)$. Making use of Eq. (26), examination of Eqs. (19)–

(25) shows that the radial flow velocity is necessarily $V_r^0(r)=0$. We further assume that the axial flow velocity satisfies

$$V_z^0(r)=V_b=\text{const}, \tag{27}$$

whereas the azimuthal flow velocity $V_\theta^0(r)$ is generally allowed to be nonzero. The assumption in Eq. (27) is consistent provided the space-charge-induced electrostatic potential energy variation over the transverse beam profile is negligible in comparison to the average axial particle kinetic energy, i.e., $(1/2)mV_b^2 \gg Z_i e[\phi^0(0)-\phi^0(r_b)]$, where r_b is the characteristic beam radius. In addition, the parallel pressure $P_\parallel^0(r)$ can have general r dependence, whereas the perpendicular pressure $P_\perp^0(r)$ is related to $V_\theta^0(r)$, $n^0(r)$ and $\phi^0(r)$ by the radial force balance equation (20). Introducing the cyclotron frequency ω_c and the equilibrium angular rotation velocity $-\omega_r(r)$ defined by

$$\omega_c=\frac{Z_i e B_f}{mc}, \qquad -\omega_r(r)=\frac{V_\theta^0(r)}{r}, \tag{28}$$

it is readily shown that Eq. (20) reduces to

$$n^0[\omega_r(\omega_c-\omega_r)+\omega_f^2]r+\frac{1}{m}\frac{\partial}{\partial r}P_\perp^0=-n^0\frac{\partial}{\partial r}\left(\frac{Z_i e\phi^0}{m}\right) \tag{29}$$

for $\partial/\partial t=\partial/\partial\theta=\partial/\partial z=0$. The sign convention for ω_r in Eqs. (28) and (29) is chosen so that the equilibrium angular rotation velocity ω_r is positive for positive ion charge species $(Z_i e>0)$ with $V_\theta^0<0$. Furthermore, Poisson's equation (25) for $\phi^0(r)$ becomes

$$\frac{1}{r}\frac{\partial}{\partial r}r\frac{\partial}{\partial r}\left(\frac{Zie\phi^0}{m}\right)=-\frac{4\pi Z_i^2 e^2}{m}n^0(r). \tag{30}$$

Equations (27), (29), and (30) constitute the final equilibrium equation within the context of the assumptions enumerated in Sec. II. Note that Eq. (29) represents a radial force balance between the inward (focusing) forces due to the axial magnetic field and the fixed background charge (the terms proportional to $\omega_c\omega_r$ and ω_f^2) and the outward (defocusing) forces due to the centrifugal, pressure-gradient and space-charge forces on a fluid element (the terms proportional to ω_r^2, $\partial P_\perp^0/\partial r$ and $\partial\phi^0/\partial r$, respectively). It is also evident that the functional form of any two of the profiles for $\omega_r(r)$, $n^0(r)$, $P_\perp^0(r)$, and $\phi^0(r)$ can be specified, and the remaining two profiles calculated self-consistently from Eqs. (29) and (30). That is, there is considerable latitude in the choice of equilibrium profiles consistent with Eqs. (29) and (30). It should also be pointed out that the special case where $\omega_r(r)=\hat{\omega}_r=\text{const}$ corresponds to a *rigid-rotor* equilibrium, which has been extensively investigated in the literature using a kinetic model based on the Vlasov–Maxwell equations.[1] We now illustrate the application of Eqs. (29) and (30) to specific examples of self-consistent equilibrium profiles.

1. Thermal equilibrium

In thermal equilibrium, the angular velocity profile $\omega_r(r)$ is constant (independent of r),

$$\omega_r(r)=\hat{\omega}_r=\text{const}, \tag{31}$$

and the perpendicular pressure profile $P_\perp^0(r)$ has the form

$$P_\perp^0(r)=n^0(r)\hat{T}_\perp, \tag{32}$$

where $\hat{T}_\perp=\text{const}$ is the temperature (in energy units). Substituting Eqs. (31) and (32) into Eq. (29) and integrating with respect to r gives

$$n_b^0(r)=\hat{n}\exp\left(-\frac{m}{2\hat{T}_\perp}\left\{[\hat{\omega}_r(\omega_c-\hat{\omega}_c)+\omega_f^2]r^2+\frac{2Z_i e}{m}\phi^0(r)\right\}\right). \tag{33}$$

Here, $\hat{n}=n^0(r=0)$ is the on-axis density, and $\phi^0(r=0)=0$ has been assumed without loss of generality. Equation (33) can be substituted into Eq. (30), and Poisson's equation integrated numerically to determine the self-consistent profiles for $\phi^0(r)$ and $n^0(r)$. This has been done in other publications,[1,2,29,30] and the results won't be repeated here except to note that for appropriate range of rotational parameter $\hat{\omega}_r$ and on-axis beam density $\hat{n}$, the density profile $n^0(r)$ in Eq. (33) is bell-shaped, assuming its maximum value $(\hat{n})$ on-axis. Furthermore, the characteristic beam radius r_b (assumed to be small in comparison with the wall radius r_w) can be many times the thermal Debye length $\lambda_D=(\hat{T}_\perp/4\pi Z_i^2 e^2\hat{n})^{1/2}$, with nearly flat density profile $(n^0\simeq\hat{n})$ in the beam interior, and with $n^0(r)$ decreasing to exponentially small values over a scale length comparable to λ_D in the outer surface region of the beam.

2. Warm-fluid Kapchinskij–Vladimirskij (KV) equilibrium

As a second example, we consider the case where the density profile $n^0(r)$ has the form of the step-function

$$n^0(r)=\begin{cases}\hat{n}=\text{const}, & 0\leq r<r_b,\\ 0, & r_b<r\leq r_w,\end{cases} \tag{34}$$

and the perpendicular pressure profile has the parabolic form described by

$$P_\perp^0(r)=\begin{cases}\hat{n}\hat{T}_\perp\left(1-\dfrac{r^2}{r_b^2}\right), & 0\leq r<r_b,\\ 0, & r_b<r\leq r_w.\end{cases} \tag{35}$$

Here, $r_b=\text{const}$ is the beam radius, $\hat{n}=\text{const}$ is the density in the beam interior, and $\hat{T}_\perp=\text{const}$ is the effective perpendicular temperature in energy units on axis $(r=0)$. From Eq. (34), note that the number of particles per unit axial length, $N=2\pi\int_0^{r_w}dr\,rn^0(r)$, can be expressed as

$$N=\pi r_b^2\hat{n} \tag{36}$$

for the step-function density profile in Eq. (34). Substituting Eq. (34) into Eq. (30), Poisson's equation can be integrated to give

$$\phi^0(r)=\begin{cases} -Z_i eN\,\dfrac{r^2}{r_b^2}, & 0\leqslant r<r_b, \\ -Z_i eN\left[1+2\ln\left(\dfrac{r}{r_b}\right)\right], & r_b<r\leqslant r_w. \end{cases} \tag{37}$$

Here, N is related to the plasma frequency-squared in the beam interior, $\hat{\omega}_p^2\equiv 4\pi Z_i^2 e^2\hat{n}/m$, by $Z_i^2e^2N/mr_b^2\equiv\hat{\omega}_p^2/4$. Without loss of generality, the constant occurring in Eq. (7) has been taken to be $\phi^0(r=r_w)=-Z_ieN[1+2\ln(r_w/r_b)]$. Substituting Eqs. (34), (35), and (37) into the radial force balance equation (29) then gives

$$\hat{\omega}_r(\omega_c-\hat{\omega}_r)+\omega_f^2-\frac{2\hat{T}_\perp/m}{r_b^2}=\frac{2Z_i^2e^2N_b}{mr_b^2}=\frac{\hat{\omega}_p^2}{2}, \tag{38}$$

in the region where $n^0(r)$ is nonzero. From Eq. (38), note that $\omega_r(r)=\hat{\omega}_r=\text{const}$ (independent of r), corresponding to a *rigid-rotor* equilibrium. The quantity $\hat{\omega}_r$ can be related directly to the average canonical angular momentum $\langle P_\theta\rangle$ defined by

$$\langle P_\theta\rangle=\frac{2\pi\int_0^{r_w}dr\ rP_\theta^0 n^0(r)}{2\pi\int_0^{r_w}dr\ rn^0(r)}, \tag{39}$$

where $P_\theta^0=mr(V_\theta^0+r\omega_c/2)$ is the canonical angular momentum of a fluid element, and $V_\theta^0(r)=-\hat{\omega}_r r$. Substituting Eq. (34) into Eq. (39) readily gives

$$\langle P_\theta\rangle=-m\left(\hat{\omega}_r-\frac{\omega_c}{2}\right)\frac{r_b^2}{2}. \tag{40}$$

That is, $\langle P_\theta\rangle=0$ whenever the beam is rotating *exactly* at the Larmor frequency ($\hat{\omega}_r=\omega_c/2$).

The profiles in Eqs. (34), (35), and (37) all have the familiar signature of the KV beam equilibrium,[10] considered here in the context of a warm-fluid model. Indeed, the force-balance equation (38) can be cast into the form of the familiar envelope equation[1,2,21,24] for a KV beam in the smooth-beam approximation ($r_b=\text{const}$). In this regard, we introduce the self-field perveance K, the unnormalized transverse emittance ϵ_d associated with the *directed* azimuthal motion (relative to the Larmor frequency), the unnormalized transverse thermal emittance ϵ_{th}, and the focusing coefficient κ_f defined by

$$\begin{aligned} K&=\frac{2NZ_i^2e^2}{mV_b^2}=\frac{r_b^2\hat{\omega}_p^2}{2V_b^2}, \\ \epsilon_d^2&=\left(\frac{2\langle P_\theta\rangle}{mV_b}\right)^2, \\ \epsilon_{\text{th}}^2&=\frac{2\hat{T}_\perp r_b^2}{mV_b^2}, \\ \kappa_f&=\left(\frac{\omega_c}{2V_b}\right)^2+\left(\frac{\omega_f}{V_b}\right)^2. \end{aligned} \tag{41}$$

Here, V_b is the average axial velocity of the beam, K is the dimensionless self-field perveance, the unnormalized emittances ϵ_d and ϵ_{th} have dimensions of length, and the focusing coefficient κ_f has dimensions of $(\text{length})^{-2}$. Making use of Eqs. (40) and (41), the radial force balance equation (38) can be expressed in the compact form

$$\kappa_f r_b-\frac{K}{r_b}-\frac{\epsilon_d^2+\epsilon_{\text{th}}^2}{r_b^3}=0. \tag{42}$$

Equation (42) is identical in form to the familiar envelope equation[1,2,21,24] for a constant-radius KV beam. Note that $\epsilon^2=\epsilon_d^2+\epsilon_{\text{th}}^2$ plays the role of a *total* effective emittance-squared in Eq. (42). Moreover, whenever the beam rotates at exactly the Larmor frequency ($\hat{\omega}_r=\omega_c/2$), then $\langle P_\theta\rangle=0$ and $\epsilon_d=0$. In this case, the only emittance contribution in Eq. (42) is ϵ_{th}^2, which is proportional to the on-axis perpendicular temperature $\hat{T}_\perp$.

3. Warm-fluid waterbag equilibrium

As a third and final equilibrium example, we consider the radial force balance equation (29) in circumstances where $\omega_r(r)=\hat{\omega}_r=\text{const}$, and the perpendicular pressure profile $P_\perp^0(r)$ is assumed to have the double-adiabatic form

$$P_\perp^0(r)=\frac{\hat{T}_\perp}{\hat{n}}\,[n^0(r)]^2. \tag{43}$$

Here, the constants $\hat{n}$ and $\hat{T}_\perp$ are the on-axis ($r=0$) values of plasma density and effective temperature (in energy units), respectively. We substitute Eq. (43) into Eq. (29), and eliminate $\partial\phi^0/\partial r$ by means of Eq. (30). Operating with $r^{-1}(\partial/\partial r)r\cdots$ then gives the closed differential equation

$$\frac{1}{r}\frac{\partial}{\partial r}\,r\,\frac{\partial}{\partial r}\frac{n^0(r)}{\hat{n}}-\frac{1}{\lambda_{\text{D}}^2}\left[\frac{n^0(r)}{\hat{n}}-\frac{\hat{\omega}_r(\omega_c-\hat{\omega}_r)+\omega_f^2}{\hat{\omega}_p^2/2}\right]=0 \tag{44}$$

for the equilibrium density profile $n^0(r)$. In Eq. (44), $\lambda_{\text{D}}=(2\hat{T}_\perp/4\pi Z_i^2e^2\hat{n})^{1/2}$ is an effective Debye length, and $\hat{\omega}_p=(4\pi Z_i^2e^2\hat{n}/m)^{1/2}$ the on-axis plasma frequency. Equation (44) is a (linear) inhomogeneous Bessel's equation for $n^0(r)$ in the beam interior.[2,28] Solving Eq. (44) for $n^0(r)$, we obtain

$$n^0(r)=\begin{cases} \hat{n}\,\dfrac{I_0(r_b/\lambda_{\text{D}})-I_0(r/\lambda_{\text{D}})}{I_0(r_b/\lambda_{\text{D}})-1}, & 0\leqslant r<r_b, \\ 0, & r_b<r\leqslant r_w. \end{cases} \tag{45}$$

Here, $I_0(x)$ is the modified Bessel function of the first kind of order zero, and the normalized beam radius r_b/λ_{D} is determined self-consistently from

$$I_0(r_b/\lambda_{\text{D}})=1+\frac{\hat{\omega}_p^2/2}{\hat{\omega}_r\omega_c-\hat{\omega}_r^2+\omega_f^2-\hat{\omega}_p^2/2}. \tag{46}$$

Note from Eq. (45) that the density profile $n^0(r)$ decreases monotonically from $\hat{n}$ at $r=0$ to zero at the outer edge of the beam ($r=r_b$). Note also from Eq. (46), that $\hat{\omega}_r\omega_c-\hat{\omega}_r^2+\omega_f^2\geqslant\hat{\omega}_p^2/2$ is required for existence of the equilibrium.

Moreover, the beam radius r_b is large in comparison with the Debye length λ_D whenever $\hat{\omega}_r\omega_c - \hat{\omega}_r^2 + \omega_f^2$ is ''closely tuned'' to $\hat{\omega}_p^2/2$.

That completes the summary of selected equilibrium examples. Clearly, a wide variety of warm-beam equilibria can be constructed consistent with Eqs. (27), (29), and (30), and the assumptions enumerated in Sec. II. Moreover, it should be kept in mind that the functional form of the parallel pressure profile $P_\parallel^0(r)$ can be specified arbitrarily for the case of axisymmetric beam propagation with $\partial/\partial\theta = 0$ and $\partial/\partial z = 0$.

B. Linearized equations

We now make use of Eqs. (19)–(25) to investigate the evolution of small-amplitude perturbations about the equilibrium profiles described by Eqs. (27), (29), and (30). All quantities are expressed as an equilibrium value (ψ^0) plus a perturbation ($\delta\psi$), i.e., $\psi(\mathbf{x},t) = \psi^0(r) + \delta\psi(\mathbf{x},t)$, where

$$\delta\psi(\mathbf{x},t) = \sum_{l=-\infty}^{\infty} \sum_{k_z=-\infty}^{\infty} \delta\psi^l(r,k_z,\omega)\exp[i(l\theta + k_z z - \omega t)]. \tag{47}$$

Here l is the azimuthal mode number, $k_z = 2\pi n/L$ is the axial wave number, where n is an integer and L is the fundamental axial periodicity length of the perturbation, and ω is the complex oscillation frequency, with $\mathrm{Im}\,\omega > 0$ corresponding to instability (temporal growth). We expand the perturbations according to Eq. (47) in Eqs. (19)–(25), and linearize for small-amplitude perturbations about the equilibrium profiles $n^0(r), \mathbf{V}^0 = -\omega_r(r) r\hat{\mathbf{e}}_\theta + V_b\hat{e}_z$, $P_\perp^0(r)$, $P_\parallel^0(r)$, and $\phi^0(r)$. Some straightforward algebra in cylindrical coordinates gives

$$-i\Omega\,\delta n^l + \frac{1}{r}\frac{\partial}{\partial r}(r n^0 \delta V_r^l) + \frac{il}{r} n^0 \delta V_\theta^l + i k_z n^0 \delta V_z^l = 0, \tag{48}$$

$$-i\Omega n^0 \delta V_r^l - (\omega_c - 2\omega_r) n^0 \delta V_\theta^l = -\frac{1}{m}\left(\frac{\partial}{\partial r}\delta P_\perp^l - \frac{\delta n^l}{n^0}\frac{\partial}{\partial r}P_\perp^0\right) - \frac{Z_i e}{m} n^0 \frac{\partial}{\partial r}\delta\phi^l, \tag{49}$$

$$-i\Omega n^0 \delta V_\theta^l + \left[\omega_c - \frac{1}{r}\frac{\partial}{\partial r}(r^2\omega_r)\right] n^0 \delta V_r^l = -\frac{1}{m}\frac{il}{r}\delta P_\perp^l - \frac{Z_i e}{m}\frac{il}{r} n^0 \delta\phi^l, \tag{50}$$

$$-i\Omega n^0 \delta V_z^l = -\frac{1}{m} i k_z \delta P_\parallel^l - \frac{Z_i e}{m} i k_z n^0 \delta\phi^l, \tag{51}$$

$$-i\Omega\,\delta P_\perp^l + \frac{\partial P_\perp^0}{\partial r}\delta V_r^l + 2P_\perp^0\left(\frac{1}{r}\frac{\partial}{\partial r} r\,\delta V_r^l + \frac{il}{r}\delta V_\theta^l + i k_z \delta V_z^l\right) - i k_z P_\perp^0 \delta V_z^l = 0, \tag{52}$$

$$-i\Omega\,\delta P_\parallel^l + \frac{\partial P_\parallel^0}{\partial r}\delta V_r^l + P_\parallel^0\left(\frac{1}{r}\frac{\partial}{\partial r} r\,\delta V_r^l + \frac{il}{r}\delta V_\theta^l + i k_z \delta V_z^l\right) + 2 i k_z P_\parallel^0 \delta V_z^l = 0, \tag{53}$$

$$\left(\frac{1}{r}\frac{\partial}{\partial r} r \frac{\partial}{\partial r} - \frac{l^2}{r^2} - k_z^2\right)\delta\phi^l = -4\pi Z_i e\,\delta n^l. \tag{54}$$

In Eqs. (48)–(51), we have introduced the Doppler-shifted complex oscillation frequency Ω defined by

$$\Omega \equiv \omega + l\omega_r - k_z V_b. \tag{55}$$

Equations (48)–(54) constitute the final set of linearized equations in the present warm-fluid model. As a general remark, keep in mind that the equilibrium profiles for $\omega_r(r)$, $n^0(r)$, $P_\perp^0(r)$, and $\phi^0(r)$ are related self-consistently by the equilibrium radial force balance equation (29) and Poisson's equation (30). In this regard, in obtaining Eq. (49), we have made use of Eq. (29) to simplify the term proportional to $\delta n^l \partial P_\perp^0/\partial r$ on the right-hand side of Eq. (49). An analysis of Eqs. (48)–(54) proceeds in the following manner. The perturbed pressures, $\delta P_\perp^l$ and $\delta P_\parallel^l$, are first calculated in terms of δV_r^l and δV_θ^l and δV_z^l from Eqs. (52) and (53) and then substituted in the linearized force balance equations (49)–(51). Equations (48)–(51) are then used to determine the perturbed flow velocity components, δV_r^l, δV_θ^l, and δV_z^l, in terms of the perturbed potential $\delta\phi^l$, and the results used in the continuity equation (48) to express δn^l in terms of $\delta\phi^l$. Equation (48) then becomes an eigenvalue equation for $\delta\phi^l(r)$ and the complex oscillation frequency ω. The eigenvalue equation for $\delta\phi^l(r)$ must be solved (often numerically) subject to the requirement that $\delta\phi^l(r)$ be regular at the origin ($r = 0$) and continuous over the interval $0 \leq r \leq r_w$, where r_w is the radius of the conducting wall. Assuming that the wall is perfectly conducting, we further require that the tangential electric field be zero at $r = r_w$, i.e., $\delta E_z^l(r = r_w) = 0 = \delta E_\theta^l(r = r_w)$, which gives the boundary condition [see Eq. (7)]

$$\delta\phi^l(r = r_w) = 0. \tag{56}$$

We now make use of Eqs. (48)–(54) to establish the appropriate eigenvalue equation for the two limiting cases analyzed in Secs. IV and V.

C. Cold-beam eigenvalue equation

We first simplify Eqs. (48)–(54) in the cold-beam limit where $P_\perp^0(r) = 0 = P_\parallel^0(r)$. In this case, $\delta P_\perp^l = 0 = \delta P_\parallel^l$ follows from Eqs. (52) and (53), and the equilibrium radial force balance equation (29) reduces to

$$[\omega_r(\omega_c - \omega_r) + \omega_f^2] r = \frac{4\pi Z_i^2 e^2}{m}\frac{1}{r}\int_0^r dr'\; r' n^0(r') \tag{57}$$

in the region where $n^0(r)$ is nonzero. Here, use has been made of Eq. (30) to eliminate $\partial\phi^0/\partial r$ in favor of $\int_0^r dr\; r n^0(r)$. Substituting $P_\perp^0 = 0 = P_\parallel^0$ and $\delta P_\perp^l = 0 = \delta P_\parallel^l$ into Eqs. (49)–(51), and solving for δV_r^l, δV_θ^l, and δV_z^l in

terms of the perturbed potential $\delta\phi^l$, the linearized continuity-Poisson equations (48) and (54) can be combined to give[47]

$$\frac{1}{r}\frac{\partial}{\partial r}\left[r\left(1-\frac{\omega_p^2}{\Gamma^2}\right)\frac{\partial}{\partial r}\,\delta\phi^l\right]-\frac{l^2}{r^2}\left(1-\frac{\omega_p^2}{\Gamma^2}\right)\delta\phi^l$$
$$-k_z^2\left(1-\frac{\omega_p^2}{\Omega^2}\right)\delta\phi^l=-\frac{l\,\delta\phi^l}{r}\frac{1}{\Omega}\frac{\partial}{\partial r}\left[\frac{\omega_p^2}{\Gamma^2}\,(\omega_c-2\omega_r)\right]. \tag{58}$$

Here, $\omega_p^2(r)=4\pi Z_i^2 e^2 n^0(r)/m$ is the local plasma frequency-squared, the equilibrium profiles for $\omega_r(r)$ and $n^0(r)$ are related self-consistently by the radial force balance equation (57), and $\Gamma^2(r,\omega)$ is defined by

$$\Gamma^2(r,\omega)\equiv\Omega^2-(\omega_c-2\omega_r)\left[\omega_c-\frac{1}{r}\frac{\partial}{\partial r}\,(r^2\omega_r)\right]. \tag{59}$$

The cold-beam eigenvalue equation (58) can be solved numerically for a broad range of choices of density profile $n^0(r)$, and analytically for the choice of step-function density profile in Eq. (34). Note that the right-hand side of Eq. (58) vanishes identically whenever $l=0$ (azimuthally symmetric perturbations) or whenever $\omega_r=\omega_c/2$, corresponding to a rigid rotation of the beam equilibrium at the Larmor frequency. Here, keep in mind that $\omega_r=\omega_c/2$ is equivalent to $\langle P_\theta\rangle=0$ [see Eq. (40)].

The cold-beam eigenvalue equation (58) will be analyzed in Sec. IV for the special case where $n^0(r)$ is a step-function density profile.

D. Warm-beam eigenvalue equation for axisymmetric flute perturbations with $l=0$ and $k_z=0$

We now simplify Eqs. (48)–(54) for the case of axisymmetric flute perturbations with $\partial/\partial\theta=0=\partial/\partial z$. Substituting $l=0$ and $k_z=0$, Eqs. (48)–(54) become

$$-i\omega\delta n+\frac{1}{r}\frac{\partial}{\partial r}\,(rn^0\delta V_r)=0, \tag{60}$$

$$-i\omega n^0\delta V_r-(\omega_c-2\omega_r)n^0\delta V_\theta$$
$$=-\frac{1}{m}\left(\frac{\partial}{\partial r}\,\delta P_\perp-\frac{\delta n}{n^0}\frac{\partial}{\partial r}\,P_\perp^0\right)-\frac{Z_i e}{m}\,n^0\,\frac{\partial}{\partial r}\,\delta\phi, \tag{61}$$

$$-i\omega n^0\delta V_\theta+\left[\omega_c-\frac{1}{r}\frac{\partial}{\partial r}\,(r^2\omega_r)\right]n^0\delta V_r=0, \tag{62}$$

$$-i\omega n^0\delta V_z=0, \tag{63}$$

$$-i\omega\delta P_\perp=-\frac{\partial P_\perp^0}{\partial r}\,\delta V_r-2P_\perp^0\frac{1}{r}\frac{\partial}{\partial r}\,r\delta V_r, \tag{64}$$

$$-i\omega\delta P_\parallel=-\frac{\partial P_\parallel^0}{\partial r}\,\delta V_r-P_\parallel^0\frac{1}{r}\frac{\partial}{\partial r}\,r\delta V_r, \tag{65}$$

$$\frac{1}{r}\frac{\partial}{\partial r}\,r\,\frac{\partial}{\partial r}\,\delta\phi=-4\pi Z_i e\,\delta n. \tag{66}$$

Here, we have dropped the superscript l notation for the $l=0$ perturbations. Note from Eq. (63) that $\delta V_z=0$. Moreover, although $\delta P_\parallel$ is generally nonzero from Eq. (65), the perturbed parallel pressure is not required in the self-consistent determination of δV_r required in the continuity equation (60). Also, keep in mind that the equilibrium profiles for $\omega_r(r)$, $P_\perp^0(r)$, and $n^0(r)$ occurring in Eqs. (60)–(65) are related self-consistently by the radial force balance equation (29) and the Poisson equation (30).

We make use of Eqs. (60), (62), and (64) to eliminate δn, δV_θ, and $\delta P_\perp$, respectively, in favor of δV_r, and substitute the resulting expressions into the linearized radial force balance equation (61) for δV_r. Some straightforward algebraic manipulation gives

$$\left\{\omega^2-(\omega_c-2\omega_r)\left[\omega_c-\frac{1}{r}\frac{\partial}{\partial r}\,(r^2\omega_r)\right]\right\}n^0\delta V_r$$
$$=-\frac{1}{m}\left\{\frac{\partial}{\partial r}\left(\delta V_r\frac{\partial}{\partial r}\,P_\perp^0\right)+\frac{\partial}{\partial r}\left(2\frac{P_\perp^0}{r}\frac{\partial}{\partial r}\,r\delta V_r\right)\right.$$
$$\left.-\frac{1}{n^0 r}\frac{\partial P_\perp^0}{\partial r}\frac{\partial}{\partial r}\,(rn^0\delta V_r)\right\}-\frac{i\omega Z_i e}{m}\,n^0\,\frac{\partial}{\partial r}\,\delta\phi. \tag{67}$$

Equation (67) provides a direct relation between the perturbed radial flow velocity δV_r and the perturbed electrostatic potential $\delta\phi$. A second relation between δV_r and $\delta\phi$ can be obtained from Eqs. (60) and (66), which can be combined to give

$$\frac{1}{r}\frac{\partial}{\partial r}\,r\,\frac{\partial}{\partial r}\,\delta\phi=\frac{4\pi i Z_i e}{\omega}\frac{1}{r}\frac{\partial}{\partial r}\,rn^0\delta V_r. \tag{68}$$

For present purposes, it is assumed that the density profile $n^0(r)$ extends from $r=0$ to an outer radius $r=r_b$, and that $n^0(r)=0$ in the vacuum region $r_b<r\leq r_w$. Integrating Eq. (68) once with respect to r then gives

$$\frac{\partial}{\partial r}\,\delta\phi=\frac{4\pi i Z_i e}{\omega}\,n^0\delta V_r,\quad 0\leq r<r_b, \tag{69}$$

in the beam interior. Here, we have set the constant of integration equal to zero in Eq. (69) because of the requirement that $\delta\phi(r)$ be regular at $r=0$. On the other hand, in the vacuum region where $n^0(r)$ and δn are zero, Eq. (68) [or Eq. (66)] can be integrated to give

$$\frac{\partial}{\partial r}\,\delta\phi=\frac{A}{r},\quad r_b<r\leq r_w, \tag{70}$$

where $A=$const. Of course $\delta\phi(r)$ must be continuous at $r=r_b$, and any discontinuity in $(\partial/\partial r)\delta\phi$ at $r=r_b$ is related to the surface-charge perturbation at $r=r_b$ by the jump condition

$$\left[\frac{\partial}{\partial r}\,\delta\phi\right]_{r_b(1+\epsilon)}-\left[\frac{\partial}{\partial r}\,\delta\phi\right]_{r_b(1-\epsilon)}$$
$$=-\frac{4\pi Z_i e}{r_b}\int_{r_b(1-\epsilon)}^{r_b(1+\epsilon)}dr\;r\,\delta n$$
$$=-\frac{4\pi i Z_i e}{\omega}\,[n^0\delta V_r]_{r_b(1-\epsilon)} \tag{71}$$

in the limit $\epsilon \to 0^+$. Here, use has been made of Eqs. (66) and (68) to obtain Eq. (71). Substituting Eqs. (69) and (70) on the left-hand side of Eq. (71) readily gives the condition $A=0$. It therefore follows from Eq. (70) that the perturbed radial electric field is zero in the vacuum region, i.e.,

$$\frac{\partial}{\partial r}\,\delta\phi = 0, \quad r_b < r \leqslant r_w, \tag{72}$$

for the class of axisymmetric flute perturbations with $l=0$ and $k_z=0$ considered here.

We therefore conclude that Eq. (69) is a valid expression for $(\partial/\partial r)\delta\phi$ over the entire interval $0 \leqslant r \leqslant r_w$, including the vacuum region where $n^0(r)=0$. Substituting Eq. (69) into Eq. (67) then gives the closed eigenvalue equation for δV_r,

$$\left\{\omega^2-(\omega_c-2\omega_r)\left[\omega_c-\frac{1}{r}\frac{\partial}{\partial r}(r^2\omega_r)\right]-\omega_p^2(r)\right\}n^0\delta V_r$$
$$=-\frac{1}{m}\left\{\frac{\partial}{\partial r}\left(\delta V_r\frac{\partial}{\partial r}P_\perp^0\right)+\frac{\partial}{\partial r}\left(2\frac{P_\perp^0}{r}\frac{\partial}{\partial r}r\,\delta V_r\right)\right.$$
$$\left.-\frac{1}{n^0 r}\frac{\partial P_\perp^0}{\partial r}\frac{\partial}{\partial r}(rn^0\delta V_r)\right\}. \tag{73}$$

Here, $\omega_p^2(r)=4\pi Z_i^2 e^2 n^0(r)/m$ is the local plasma frequency-squared. Equation (73) is the final form of the eigenvalue equation for axisymmetric flute perturbations with $l=0$ and $k_z=0$ using the warm-beam fluid model developed in Sec. II. As noted earlier, Eq. (73) is valid for general equilibrium profiles $\omega_r(r)$, $n^0(r)$, and $P_\perp^0(r)$ consistent with the radial force balance equation (29) and Poisson's equation (30). The advantage of having integrated the continuity equation (60) and Poisson's equation (66) to obtain the relation in Eq. (69) is evident. The eigenvalue equation (73) for δV_r is second order (with respect to the r derivatives), whereas the analogous eigenvalue equation for $\delta\phi$ when thermal effects are included would be third order.

Equation (73) will be used in Sec. V to investigate detailed stability properties for the choice of step-function density profile and parabolic pressure profile in Eqs. (34) and (35).

IV. COLD-BEAM STABILITY PROPERTIES

The cold-beam eigenvalue equation (58), derived for the case of zero transverse and longitudinal equilibrium pressures [i.e., $P_\perp^0(r)=0=P_\parallel^0(r)$], can be used to investigate detailed stability properties for a wide range of equilibrium density profiles $n^0(r)$ and angular velocity profiles $\omega_r(r)$ consistent with the cold-fluid radial force balance equation (57). For present purposes, we consider the case where $n^0(r)$ has the step-function profile in Eq. (34) and Fig. 1. This simple case, corresponding to a cold KV beam equilibrium with $\hat{T}_\perp=0$, allows analytical progress and can be physically motivated. In many intense-beam applications, the thermal emittance $\epsilon_{\rm th}$ is small and the transverse density profile is approximately uniform over a distance of many thermal Debye lengths $\lambda_{\rm D}$ out to some radius $r_b(\gg\lambda_{\rm D})$, where the density falls abruptly to zero over a few Debye lengths. In such instances, the fluid modes predicted by this cold-beam model should be similar to those of realistic beam distributions.

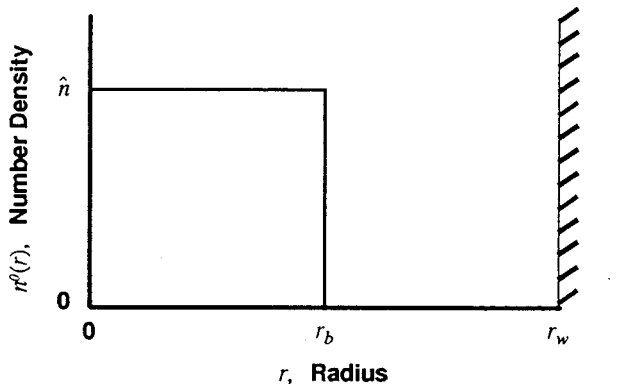

FIG. 1. Equilibrium density profile $n^0(r)$ is plotted as a function of radius r for a step-function density profile. A perfectly conducting, cylindrical wall is located at $r=r_w$.

For a cold beam with step-function density profile, $\hat{T}_\perp=0$ and the equilibrium force balance equation (57) reduces to the simple condition

$$\hat{\omega}_r(\omega_c-\hat{\omega}_r)+\omega_f^2=\frac{\hat{\omega}_p^2}{2} \tag{74}$$

in the beam interior $(0 \leqslant r < r_b)$. Here, $\hat{\omega}_p^2=4\pi\hat{n}Z_i^2e^2/m$, where $n^0(r)=\hat{n}=$const and $\omega_r(r)=\hat{\omega}_r=$const are the equilibrium density and angular rotation velocity in the interval $0 \leqslant r < r_b$. Equation (74) can be solved for the angular rotation velocity to give

$$\hat{\omega}_r=\frac{\omega_c}{2}\pm\left[\left(\frac{\omega_c}{2}\right)^2+\omega_f^2-\frac{\hat{\omega}_p^2}{2}\right]^{1/2}. \tag{75}$$

For existence of the equilibrium, it follows from Eq. (75) that the inequality

$$s_e \equiv \frac{2\hat{\omega}_p^2}{\omega_c^2+4\omega_f^2} \leqslant 1 \tag{76}$$

is required, where s_e is a positive, dimensionless measure of space-charge strength. For $s_e>1$, radially confined equilibria do not exist because the defocusing self-field force proportional to $\hat{\omega}_p^2/2$ is too large for the beam to be radially confined by the net focusing force proportional to $(\omega_c/2)^2+\omega_f^2$. The limiting case, $s_e \to 1$ is referred to as the Brillouin density limit and corresponds to the space-charge limit of the transport channel neglecting thermal effects. Further analysis of the equilibrium structure of a KV beam is presented in Appendix A.

For the step-function density profile in Eq. (34), the average canonical angular momentum $\langle P_\theta \rangle$ is given by Eq. (40) as $\langle P_\theta \rangle = -m(\hat{\omega}_r-\omega_c/2)r_b^2/2$. It follows that $\langle P_\theta \rangle = 0$ implies that the beam is rotating at the Larmor frequency, i.e., $\hat{\omega}_r=\omega_c/2$. Note also that Eq. (75) can be expressed in terms of the space-charge parameter s_e as

$$\hat{\omega}_r-\frac{\omega_c}{2}=\pm\frac{\hat{\omega}_p}{\sqrt{2}}\left(\frac{1-s_e}{s_e}\right)^{1/2}. \tag{77}$$

Equation (77) shows that a cold KV equilibrium with $\langle P_\theta \rangle = 0$ corresponds to the Brillouin density limit with self-field parameter $s_e = 1$, whereas $\langle P_\theta \rangle \neq 0$ corresponds to $s_e < 1$.

For the step-function density profile in Eq. (34), the cold-beam eigenvalue equation (58) reduces to[47]

$$\frac{1}{r}\frac{\partial}{\partial r}\left\{r\left[1-\frac{\omega_p^2(r)}{\Omega^2-4(\hat{\omega}_r-\omega_c/2)^2}\right]\frac{\partial}{\partial r}\,\delta\phi^l\right\} - \frac{l^2}{r^2}\left[1-\frac{\omega_p^2(r)}{\Omega^2-4(\hat{\omega}_r-\omega_c/2)^2}\right]\delta\phi^l - k_z^2\left[1-\frac{\omega_p^2(r)}{\Omega^2}\right]\delta\phi^l = -\frac{2l\,\delta\phi^l}{r}\,\frac{\hat{\omega}_p^2(\hat{\omega}_r-\omega_c/2)}{\Omega[\Omega^2-4(\hat{\omega}_r-\omega_c/2)^2]}\,\delta(r-r_b), \tag{78}$$

where $\Omega = \omega + l\hat{\omega}_r - k_z V_b$ is the Doppler-shifted oscillation frequency, $\delta(x)$ is the Dirac delta-function, and

$$\omega_p^2(r) = \begin{cases} \hat{\omega}_p^2 = \text{const}, & 0 \leq r < r_b, \\ 0, & r_b < r \leq r_w. \end{cases} \tag{79}$$

The eigenvalue equation (78) can be solved analytically because the coefficients proportional to $\omega_p^2(r)$ are constant, both inside the beam, where $\omega_p^2(r) = \hat{\omega}_p^2$, and outside the beam, where $\omega_p^2(r) = 0$. The solution that is regular at $r = 0$, continuous at $r = r_b$, and satisfies $\delta\phi^l(r = r_w) = 0$ at the conducting wall can be expressed as

$$\delta\phi^l(r) = \begin{cases} A_l J_l(Tr), & 0 \leq r < r_b, \\ A_l J_l(Tr_b)\,\dfrac{I_l(k_z r)K_l(k_z r_w) - K_l(k_z r)I_l(k_z r_\omega)}{I_l(k_z r_b)K_l(k_z r_w) - K_l(k_z r_b)I_l(k_z r_w)}, & r_b < r \leq r_w, \end{cases} \tag{80}$$

where T^2 is defined by

$$T^2 = -k_z^2\,\frac{1-\hat{\omega}_p^2/\Omega^2}{1-\hat{\omega}_p^2/[\Omega^2-4(\hat{\omega}_r-\omega_c/2)^2]}. \tag{81}$$

Here, A_l is a constant, $J_l(x)$ is the lth-order ordinary Bessel function, and $I_l(x)$ and $K_l(x)$ are lth-order modified Bessel functions of the first and second kind, respectively. The remaining boundary condition is obtained by integrating Eq. (78) across the surface of the beam at $r = r_b$. Multiplying Eq. (78) by r, and operating with $\int_{r_b(1-\epsilon)}^{r_b(1+\epsilon)} dr \cdots$, where $\epsilon \to 0^+$, readily gives

$$\left[\frac{\partial}{\partial r}\,\delta\phi^l\right]_{r=r_b(1+\epsilon)} - \left[1-\frac{\hat{\omega}_p^2}{\Omega^2-4(\hat{\omega}_r-\omega_c/2)^2}\right]\times\left[\frac{\partial}{\partial r}\,\delta\phi^l\right]_{r=r_b(1-\epsilon)} = -\frac{2l[\delta\phi^l]_{r=r_b}}{r_b}\,\frac{\hat{\omega}_p^2(\hat{\omega}_r-\omega_c/2)}{\Omega[\Omega^2-4(\hat{\omega}_r-\omega_c/2)^2]}. \tag{82}$$

Substituting Eqs. (80) into Eq. (82) and rearranging terms, we obtain the dispersion relation

$$k_z r_b\,\frac{K_l(k_z r_w)I_l'(k_z r_b) - K_l'(k_z r_b)I_l(k_z r_w)}{K_l(k_z r_w)I_l(k_z r_b) - K_l(k_z r_b)I_l(k_z r_w)} - \left[1-\frac{\hat{\omega}_p^2}{\Omega^2-4(\hat{\omega}_r-\omega_c/2)^2}\right]Tr_b\,\frac{J_l'(Tr_b)}{J_l(Tr_b)} = -2l\,\frac{\hat{\omega}_p^2(\hat{\omega}_r-\omega_c/2)}{\Omega[\Omega^2-4(\hat{\omega}_r-\omega_c/2)^2]}. \tag{83}$$

Here, a prime denotes differentiation with respect to the functional argument, i.e., $J_l'(Tr_b) = [dJ_l(x)/dx]_{x=Tr_b}$. The Bessel function recursion relations $xJ_l'(x) = lJ_l(x) - xJ_{l+1}(x)$, $xI_l'(x) = lI_l(x) + xI_{l+1}(x)$, and $xK_l'(x) = lK_l(x) - xK_{l+1}(x)$ can be used to further simplify Eq. (83) and subsequent expressions.

Often, the beam density is directly measured experimentally, whereas the potential must be inferred indirectly. Therefore, it is also useful to determine the normal-mode eigenfunction expressed in terms of the perturbed density δn. In this regard, the Poisson equation (54) and the eigenvalue equation (78) can be employed with $\delta\phi^l$ given by Eq. (80) to express the eigenfunction for $\delta n^l(r)$ as

$$\delta n^l(r) = \frac{A_l}{4\pi Z_i e}\,(k_z^2 - T^2)J_l(Tr)\Theta(r_b - r) + \frac{A_l}{4\pi Z_i e}\,\frac{\hat{\omega}_p^2}{\Omega^2-4(\hat{\omega}_r-\omega_c/2)^2}\left[Tr_b J_l'(Tr_b) + 2lJ_l(Tr_b)\,\frac{\hat{\omega}_r-\omega_c/2}{\Omega}\right]\frac{1}{r}\,\delta(r-r_b), \tag{84}$$

where $\Theta(x)$ is the Heaviside step function defined by $\Theta(x) = 1$ for $x > 0$ and $\Theta(x) = 0$ for $x < 0$. The terms in the expression for δn^l in Eq. (84) that multiply the step and delta functions correspond to ''body-wave'' and ''surface-wave'' perturbations, respectively. The surface-wave term in Eq. (84) is a singular layer of charge at the edge radius r_b of the beam that is a manifestation, within linear theory, of a small change in the edge radius of the beam. (This can be demonstrated using analogous arguments to those employed for the case of warm-beam perturbations with $k_z = 0$ and $l = 0$ in Appendix C.) Comparing Eqs. (80) and (84), note that the body-wave component ($0 \leq r < r_b$) of the cold-beam density eigenfunction, δn^l, is proportional to the potential eigenfunction $\delta\phi^l$.

The eigenfunction (80) and the dispersion relation (83) describe perturbations about a cold-beam equilibrium with step-function density profile. In general, the dispersion relation (83) is a transcendental equation which determines the Doppler-shifted oscillation frequency $\Omega=\omega+l\hat{\omega}_r-k_zV_b$ in terms of the azimuthal mode number l, the normalized axial wave number k_zr_b, the beam plasma frequency $\hat{\omega}_p$, and the shifted frequency $\hat{\omega}_r-\omega_c/2=-2\langle P_\theta\rangle/mr_b^2$. For present purposes, we analyze, in turn, properties of the solutions to Eq. (83) for zero and nonzero canonical angular momentum $\langle P_\theta\rangle$. For $\langle P_\theta\rangle=0$, the solution is described analytically. On the other hand, for $\langle P_\theta\rangle\neq 0$, the solution to Eq. (83) must generally be determined numerically. Various limiting cases, including those with multispecies generalizations and streaming instabilities, have been analyzed elsewhere.[47]

A. Beam equilibrium with zero canonical angular momentum

In Sec. III A 2, it was shown for a warm-fluid KV beam equilibrium that nonzero canonical angular momentum $\langle P_\theta\rangle$ plays the role of a directed emittance, $\epsilon_d=2|\langle P_\theta\rangle|/mV_b$. This directed emittance ϵ_d adds in quadrature with the thermal beam emittance, $\epsilon_{\rm th}=(2\hat{T}_\perp r_b^2/mV_b^2)^{1/2}$, to produce the total effective emittance-squared ϵ^2 of the beam, i.e., $\epsilon^2=\epsilon_d^2+\epsilon_{\rm th}^2$. The total emittance-squared ϵ^2 and the self-field perveance $K=\hat{\omega}_p^2r_b^2/2V_b^2$ then fix the equilibrium beam radius r_b, determined from the envelope equation (42). Larger emittance leads to increased beam radius r_b. Because of this, intense beams are usually launched from the source under conditions such that $\langle P_\theta\rangle=0$ in order to reduce the transverse beam size. Thus, the special case of a cold beam with $\langle P_\theta\rangle=0$ is of considerable practical interest.

A cold KV beam equilibrium with $\langle P_\theta\rangle=0$ necessarily rotates at the Larmor frequency with $\hat{\omega}_r=\omega_c/2$, which corresponds to the Brillouin density limit with space-charge parameter $s_e=1$. For $\hat{\omega}_r=\omega_c/2$, it follows from Eq. (81) that $T^2=-k_z^2$, and $J_l(Tr)=i^lI_l(k_zr)$. In this case, the expressions for the eigenfunction in terms of the perturbed potential [Eq. (80)] and perturbed density [Eq. (84)] reduce to

$$\delta\phi^l(r)=\begin{cases} i^lA_lI_l(k_zr), & 0\leqslant r<r_b, \\ i^lA_lI_l(k_zr_b)\,\dfrac{I_l(k_zr)K_l(k_zr_w)-K_l(k_zr)I_l(k_zr_w)}{I_l(k_zr_b)K_l(k_zr_w)-K_l(k_zr_b)I_l(k_zr_w)}, & r_b<r\leqslant r_w, \end{cases} \tag{85}$$

and

$$\delta n^l(r)=\frac{i^lA_l}{2\pi Z_ie}\,k_z^2I_l(k_zr)\Theta(r_b-r)+\frac{i^lA_l}{4\pi Z_ie}\,\frac{\hat{\omega}_p^2}{\Omega^2}\,k_zr_bI_l'(k_zr_b)\,\frac{1}{r}\,\delta(r-r_b), \tag{86}$$

respectively. The solution in Eq. (85) can also be obtained directly by noting for $\hat{\omega}_r=\omega_c/2$ that the right-hand side of the eigenvalue equation (78) vanishes, and the eigenvalue equation reduces to

$$\frac{1}{r}\,\frac{\partial}{\partial r}\left\{r\left[1-\frac{\omega_p^2(r)}{\Omega^2}\right]\frac{\partial}{\partial r}\,\delta\phi^l\right\}-\left(\frac{l^2}{r^2}+k_z^2\right)\left[1-\frac{\omega_p^2(r)}{\Omega^2}\right]\delta\phi^l=0. \tag{87}$$

Because the coefficients proportional to $\omega_p^2(r)$ in the reduced eigenvalue equation (87) are constant both inside the beam, where $\omega_p^2(r)=\hat{\omega}_p^2$, and outside the beam, where $\omega_p^2(r)=0$, Eq. (87) is of the modified Bessel form. The solution in Eq. (85) then follows trivially from the relevant boundary conditions. Similarly, after some algebraic simplifications that make use of $\hat{\omega}_r=\omega_c/2$, the dispersion relation (83) reduces to

$$\Omega^2=\hat{\omega}_p^2\,\frac{I_l'(k_zr_b)}{I_l(k_zr_w)}\left[\frac{I_l(k_zr_b)K_l(k_zr_w)-K_l(k_zr_b)I_l(k_zr_w)}{I_l(k_zr_b)K_l'(k_zr_b)-K_l(k_zr_b)I_l'(k_zr_b)}\right]. \tag{88}$$

Using the modified Bessel function Wronskian identity $I_l'(x)K_l(x)-I_l(x)K_l'(x)=1/x$, the cold-beam dispersion relation (88) can be further simplified to give

$$\Omega^2=\hat{\omega}_p^2k_zr_bI_l(k_zr_b)I_l'(k_zr_b)\left[\frac{K_l(k_zr_b)}{I_l(k_zr_b)}-\frac{K_l(k_zr_w)}{I_l(k_zr_w)}\right]. \tag{89}$$

The dispersion relation (89) determines the oscillation frequency of electrostatic perturbations about a cold KV beam equilibrium rotating at the Larmor frequency. The simple analytical form of the dispersion relation is due to the assumption that $\hat{\omega}_r=\omega_c/2$. In the long-axial-wavelength limit $k_z^2r_w^2\ll 1$, the dispersion relation (89) can be further simplified using asymptotic expressions for $I_l(x)$ and $K_l(x)$ to give

$$\Omega^2\simeq\begin{cases}\dfrac{\hat{\omega}_p^2}{2}\,(k_zr_b)^2\,\ln\left(\dfrac{r_w}{r_b}\right), & k_z^2r_w^2\ll 1 \ \text{ and } \ l=0, \\ \dfrac{\omega_p^2}{2}\left[1-\left(\dfrac{r_b}{r_w}\right)^{2l}\right], & k_z^2r_w^2\ll 1 \ \text{ and } \ l\neq 0.\end{cases} \tag{90}$$

Similarly, in the short-axial-wavelength limits $k_z^2r_w^2\gg 1,l^2$ and $k_z^2r_b^2\gg 1,l^2$, the dispersion relation (89) simplifies to give

$$\Omega^2\simeq\begin{cases}\hat{\omega}_p^2k_zr_bI_l'(k_zr_b)K_l(k_zr_b), & k_z^2r_w^2\gg 1,l^2, \\ \dfrac{\hat{\omega}_p^2}{2}, & k_z^2r_b^2\gg 1,l^2.\end{cases} \tag{91}$$

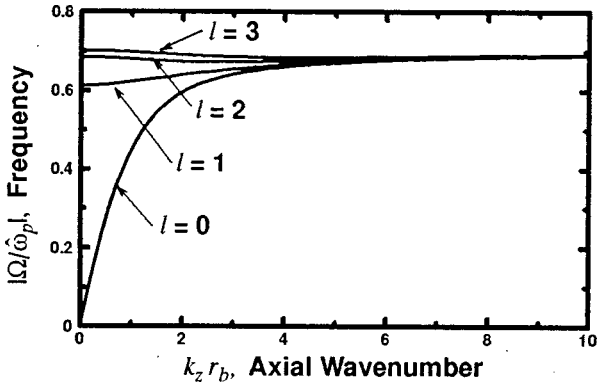

FIG. 2. Solutions for the normalized frequency $|\Omega/\hat{\omega}_p|$ of electrostatic perturbations, calculated from the cold-fluid dispersion relation (89), are plotted as a function of normalized axial wave number $k_z r_b$ for a cold KV beam equilibrium rotating at the Larmor frequency ($\hat{\omega}_r = \omega_c/2$). The ratio of beam radius to conducting walls radius is chosen to be $r_b/r_w = 0.5$, and results are shown for azimuthal mode numbers $l = 0$, 1, 2, and 3.

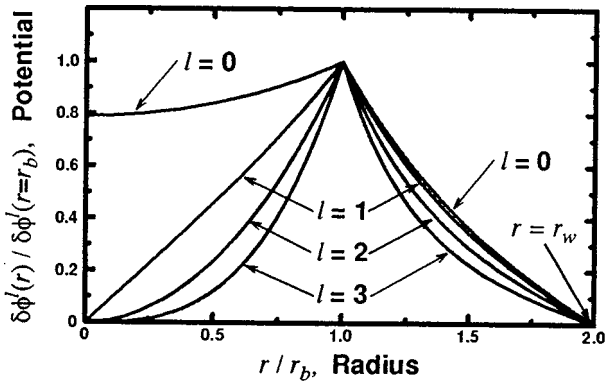

FIG. 3. Solutions for the normalized eigenfunction $\delta\phi^l/\delta\phi^l(r=r_b)$ of electrostatic perturbations, calculated from Eq. (85), are plotted as a function of normalized radial coordinate r/r_b for a cold KV beam equilibrium rotating at the Larmor frequency ($\hat{\omega}_r = \omega_c/2$). The system parameters are identical to those in Fig. 2 with $k_z r_b = 1$.

Here, $k_z^2 r_w^2 \gg 1, l^2$ is used to denote $k_z^2 r_w^2 \gg 1$ for $l = 0$ and $k_z^2 r_w^2 \gg l^2$ for $l \neq 0$, etc. Also, in Eqs. (90) and (91), note that $r_w > r_b$, so $k_z^2 r_w^2 \ll 1$ and $k_z^2 r_b^2 \gg 1$ imply that $k_z^2 r_b^2 \ll 1$ and $k_z^2 r_w^2 \gg 1$, etc. Note from Eqs. (90) and (91) that the plasma oscillations described by Eq. (89) are *dispersive*. The $l = 0$, $k_z^2 r_w^2 \ll 1$ limit in Eq. (90) is $\Omega^2 = g\hat{\omega}_p^2 (k_z r_b)^2/4$ with geometric factor $g = 2\ln(r_w/r_b)$, which corresponds to the well-known oscillation frequency for long-wavelength longitudinal perturbations in a cold beam with step-function density profile.[47] Note also, that short-wavelength perturbations with $k_z^2 r_b^2 \gg 1, l^2$ have characteristic frequency $\Omega = \pm\hat{\omega}_p/\sqrt{2}$, which is the well-known oscillation frequency of perturbations in beam radius (i.e., envelope oscillations) for a cold KV beam.[1,2]

Plots of the normalized frequency $|\Omega/\hat{\omega}_p|$, obtained from Eq. (89), versus normalized axial wave number $k_z r_b$ are presented in Fig. 2 for $0 \leq k_z r_b \leq 10$, $r_b/r_w = 0.5$, and azimuthal mode numbers $l = 0$, 1, 2, and 3. Note that there are two frequencies $\pm|\Omega|$ corresponding to each dispersion curve plotted, and the normal modes associated with these solutions are related by a phase difference. Note also from Fig. 2 that the $l \neq 0$ dispersion curves have only a weak dependence on k_z, whereas the $l = 0$ curve is strongly dependent on k_z for $k_z^2 r_b^2 \lesssim 1$. Consistent with Eq. (91), all curves approach the envelope-mode oscillation frequency $|\Omega/\hat{\omega}_p| = 1/\sqrt{2}$ in the short-wavelength limit $k_z^2 r_b^2 \gg 1, l^2$. The corresponding eigenfunctions $\delta\phi^l(r)$, normalized to $\delta\phi^l(r=r_b) = i^l A_l I_l(k_z r_b)$, are plotted versus r/r_b in Fig. 3 for r in the interval $0 \leq r \leq r_w$ and the choice of system parameters $k_z r_b = 1$, $r_b/r_w = 0.5$, and $l = 0$, 1, 2, and 3. Here, the expression for $\delta\phi^l(r)$ in Eq. (85) has been used. As the azimuthal mode number l increases, we note from Fig. 3 that the eigenfunctions $\delta\phi^l(r)$ become increasingly peaked at $r = r_b$, corresponding to a strong surface-charge perturbation at the surface of the beam. Finally, note from Eqs. (85) and (86) that $\delta\phi^l(r)/\delta\phi^l(r=r_b) = \delta n^l(r)/\delta n^l(r=r_b)$ interior to the beam ($0 \leq r < r_b$) and $\delta n^l(r) = 0$ exterior the beam ($r_b < r \leq r_w$). Therefore, the normalized potential curves in Fig. 3 serve equally well to illustrate the interior structure of the body-wave component of the density eigenfunction $\delta n^l(r)$.

B. Beam equilibrium with nonzero canonical angular momentum

Since the directed and thermal emittances, $\epsilon_d = 2|\langle P_\theta\rangle|/mV_b$ and $\epsilon_{\rm th} = (2\hat{T}_\perp r_b^2/mV_b^2)^{1/2}$ are indistinguishable in their contributions to the equilibrium envelope radius of a KV beam [see Eq. (42)], one might expect, particularly for small azimuthal mode numbers l, that these emittances also contribute in a qualitatively similar manner to the fluid modes supported by the equilibrium. In particular, one might conjecture that a *warm* KV beam with canonical angular momentum $\langle P_\theta\rangle = -m(\hat{\omega}_r - \omega_c/2)r_b^2/2 = 0$ and total emittance $\epsilon = \epsilon_{\rm th}$ might support similar mode structure to a cold KV beam with $\langle P_\theta\rangle \neq 0$ and total emittance $\epsilon = \epsilon_d$, provided the values of $\epsilon_{\rm th}$ and ϵ_d are the same.

Motivated by this conjecture, we now analyze the cold-beam dispersion relation (83) for nonzero canonical angular momentum $\langle P_\theta\rangle$. It is found that the dispersion relation describes stable electrostatic oscillations for all physically allowed equilibrium parameters. In contrast to the case $\langle P_\theta\rangle = 0$ analyzed in Sec. IV A, when $\langle P_\theta\rangle \neq 0$ and $\hat{\omega}_r \neq \omega_c/2$, it is found that analytical simplification is straightforward only in the long-axial-wavelength regime where $k_z^2 r_w^2 \ll 1$. In this limit, asymptotic expressions for the Bessel functions can be employed to show that

$$\Omega^2 \simeq \frac{\hat{\omega}_p^2}{2}(k_z r_b)^2 \ln\left(\frac{r_w}{r_b}\right), \tag{92}$$

for $k_z^2 r_w^2 \ll 1$ and $l = 0$, and

$$\Omega \simeq (\hat{\omega}_r - \omega_c/2) \pm \frac{1}{2}\left\{4\left(\hat{\omega}_r - \frac{\omega_c}{2}\right)^2 + 2\hat{\omega}_p^2\left[1 - \left(\frac{r_b}{r_w}\right)^{2l}\right]\right\}^{1/2}, \tag{93}$$

for $k_z^2 r_w^2 \ll 1$ and $l \neq 0$. Comparing Eqs. (92) and (93) for $\langle P_\theta\rangle \neq 0$ with the corresponding limits in Eq. (90) for $\langle P_\theta\rangle = 0$, it is evident that the long-wavelength $l = 0$ solutions are the same in the two cases. On the other hand, the long-wavelength $l \neq 0$ solutions are modified when $\langle P_\theta\rangle \neq 0$, i.e., when $\hat{\omega}_r \neq \omega_c/2$.

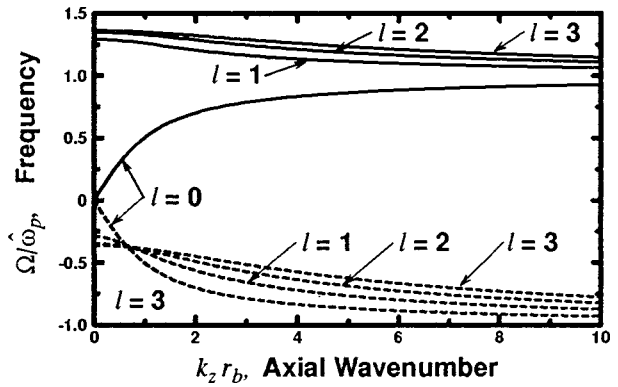

FIG. 4. Solutions for the normalized frequency $\Omega/\hat{\omega}_p$ of electrostatic perturbations, calculated from the cold-fluid dispersion relation (83), are plotted as a function of normalized axial wave number $k_z r_b$ for a cold KV beam equilibrium with $\langle P_\theta \rangle \neq 0$. System parameters correspond to $r_b/r_w = 0.5$ and $\hat{\omega}_r - \omega_c/2 = 0.5\hat{\omega}_p$, and results are shown for azimuthal mode numbers $l = 0$, 1, 2, and 3.

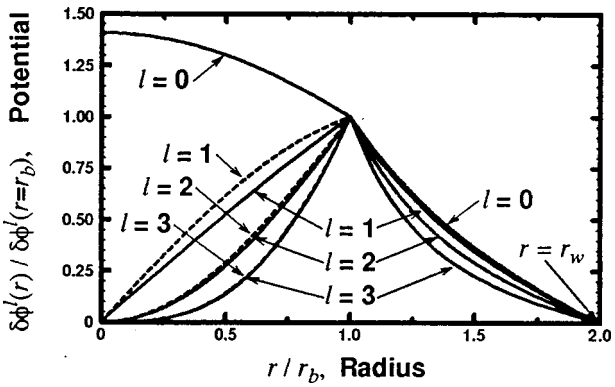

FIG. 5. Solutions for the normalized eigenfunction $\delta\phi^l/\delta\phi^l(r=r_b)$ of electrostatic perturbations, calculated from Eq. (80), are plotted as a function of normalized radial coordinate r/r_b for a cold KV beam equilibrium with $\langle P_\theta \rangle \neq 0$. The system parameters are identical to those in Fig. 4 with $k_z r_b = 1$.

The important features of the solutions to the cold-beam dispersion relation (83) with $\langle P_\theta \rangle \neq 0$ are illustrated in Fig. 4. Here the normalized frequency $\Omega/\hat{\omega}_p$, calculated numerically from Eq. (83), is plotted versus normalized axial wave number $k_z r_b$ for $0 \leqslant k_z r_b \leqslant 10$ and the choice of system parameters $r_b/r_w = 0.5$ and $\hat{\omega}_r - \omega_c/2 = 0.5\hat{\omega}_p$, and azimuthal mode numbers $l = 0$, 1, and 2. This choice of relative angular velocity, $\hat{\omega}_r - \omega_c/2 = 0.5\hat{\omega}_p$, corresponds to self-field parameter $s_e = \hat{\omega}_p^2/(\omega_c^2 + 4\omega_f^2) = 2/3$, and canonical angular momentum $\langle P_\theta \rangle = -m\hat{\omega}_p^2 r_b^2/4$. For $\langle P_\theta \rangle \neq 0$, note from Fig. 4 that the positive- (solid) and negative-frequency (dashed) branches for Ω are of equal magnitude with opposite sign for $l = 0$, whereas the magnitudes are different when $l \neq 0$. The corresponding eigenfunctions $\delta\phi^l(r)$, normalized to $\delta\phi^l(r=r_b) = A_l J_l(Tr_b)$, are plotted versus r/r_b in Fig. 5 for the same choice of system parameters as in Fig. 4 and for $k_z r_b = 1$. Here, the full expression for $\delta\phi^l(r)$ in Eq. (80) has been used. For $l \geqslant 1$, note from Fig. 5 that the normalized eigenfunctions for the positive- (solid) and negative-frequency (dashed) solutions plotted in Fig. 4 have different functional forms within the beam ($r < r_b$), whereas outside the beam ($r > r_b$), or for $l = 0$ within the beam, the normalized eigenfunctions are the same for both positive- and negative-frequency solutions. Also, comparing Eqs. (80) and (84), note that $\delta\phi^l(r)/\delta\phi^l(r=r_b) = \delta n^l(r)/\delta n^l(r=r_b)$ interior to the beam ($0 \leqslant r < r_b$) and $\delta n^l(r) = 0$ exterior the beam ($r_b < r \leqslant r_w$). Therefore, analogous to the case where $\langle P_\theta \rangle = 0$, the normalized potential curves in Fig. 5 also illustrate the interior structure of the body-wave component of the density eigenfunction $\delta n^l(r)$.

Contrasting Figs. 2 and 3 obtained for $\langle P_\theta \rangle = 0$ with the corresponding Figs. 4 and 5 obtained for $\langle P_\theta \rangle \neq 0$, it is evident that the mode frequencies and eigenfunctions for electrostatic perturbations about a cold KV beam equilibrium exhibit a sensitive dependence on canonical angular momentum. In particular, finite $\langle P_\theta \rangle$ significantly changes the mode structure. For $\langle P_\theta \rangle \neq 0$, the positive and negative mode frequencies Ω remain equal in magnitude for $l = 0$, but differ in magnitude for $l \neq 0$. This contrasts with the case $\langle P_\theta \rangle = 0$, where the positive and negative mode frequencies are equal in magnitude for all l. Moreover, the functional dependence of Ω on the normalized axial wave number $k_z r_b$ changes significantly for finite $\langle P_\theta \rangle$. Larger-magnitude frequencies $|\Omega|$ are found as $(\hat{\omega}_r - \omega_c/2)^2 \propto \langle P_\theta \rangle^2$ is increased, and the frequencies are shifted about $\Omega = 0$. Also, the normalized eigenfunctions $\delta\phi^l(r)/\delta\phi^l(r=r_b)$ differ significantly within the beam ($r < r_b$). The eigenfunction bifurcates from modified Bessel function form, i.e., $\delta\phi^l(r) \sim I_l(k_z r)$, to ordinary Bessel function form, i.e., $\delta\phi^l(r) \sim J_l(Tr)$ with T real, whenever T^2 defined in Eq. (81) satisfies $T^2 > 0$. It follows from Eqs. (81), (92), and (93) that for small $\langle P_\theta \rangle^2 \propto (\hat{\omega}_r - \omega_c/2)^2/\hat{\omega}_p^2 \ll 1$ and $k_z^2 r_w^2 \ll 1$, this bifurcation to ordinary Bessel function form occurs for azimuthal mode number $l = 0$ when $k_z^2 r_w^2 < 8(\hat{\omega}_r - \omega_c/2)^2/[\hat{\omega}_p^2 \ln(r_w/r_b)]$, and does not occur for $l \neq 0$. As $(\hat{\omega}_r - \omega_c/2)^2/\hat{\omega}_p^2$ is increased, the bifurcation threshold value of $k_z^2 r_b^2$ increases for $l = 0$, and modes with $l \neq 0$ begin to bifurcate for $k_z^2 r_b^2$ less than l-dependent threshold values. It is found numerically, for $(\hat{\omega}_r - \omega_c/2)^2/\hat{\omega}_b^2$ sufficiently large at fixed r_w/r_b, that all allowed frequencies Ω correspond to $T^2 > 0$ and $\delta\phi^l(r) \sim J_l(Tr)$, with T real for all azimuthal mode numbers l and all values of $k_z r_b$. The choice of $\langle P_\theta \rangle \neq 0$ parameters illustrated in Figs. 4 and 5 satisfy this threshold condition [for $r_b/r_w = 0.5$, all modes have $\delta\phi^l(r) \sim J_l(Tr)$, with T real for all values of l and $k_z^2 r_b^2$ when $|\hat{\omega}_r - \omega_c/2|/\hat{\omega}_p > 0.457$]. Contrasting Figs. 3 and 5, note that the ordinary Bessel function structure of the eigenfunction illustrated in Fig. 5 is less peaked at the beam edge ($r = r_b$) than for the case where the eigenfunction has modified Bessel function structure as illustrated in Fig. 3.

V. WARM-BEAM STABILITY PROPERTIES FOR AXISYMMETRIC FLUTE PERTURBATIONS ABOUT A KV BEAM EQUILIBRIUM

In all practical applications, charged particle beams have a finite velocity spread, which is represented in the present fluid model by nonzero transverse and longitudinal pressures, $P_\perp^0(r)$ and $P_\parallel^0(r)$. In a kinetic model, it is well-known that the velocity spread of the beam equilibrium can have a

strong influence on the detailed stability properties of the system. The influence of finite velocity spread on the stability behavior of the system must also be examined in the present fluid model. Further motivating this point, significant differences in mode structure were found in Sec. IV for a cold KV beam equilibrium with zero and nonzero canonical angular momentum $\langle P_\theta \rangle$. These differences, together with the conjecture that finite $\langle P_\theta \rangle$ can provide qualitatively similar effects to finite velocity spread further motivates the need for a warm-beam stability theory with nonzero pressure. The general analysis of warm-beam stability properties for $k_z \neq 0$ is complicated. Therefore, to obtain readily interpretable results, we examine the fluid stability properties of a warm KV beam equilibrium for the case of axisymmetric flute perturbations with $l=0$ and $k_z=0$. The analysis of more complicated modes with finite axial wave number ($k_z \neq 0$) is deferred to future studies.

The warm-beam eigenvalue equation (73), derived for $l=0$ and $k_z=0$, can be used to investigate transverse stability properties for a wide range of warm-beam equilibria with radial profiles for density $n^0(r)$, angular velocity $\omega_r(r)$, and perpendicular pressure $P_\perp^0(r)$ consistent with the warm-fluid radial force balance equation (29). In the present analysis, we consider the special case corresponding to a warm KV beam equilibrium, where the equilibrium density $n^0(r)$ has the step-function profile in Eq. (34) and Fig. 1, with $n^0(r)=\hat{n}=$const within the beam ($0 \leqslant r < r_b$), and the equilibrium pressure profile decreases parabolically with radius r within the beam according to $P_\perp^0(r)=\hat{n}\hat{T}_\perp(1-r^2/r_b^2)$ with $\hat{T}_\perp=$const [see Eq. (35)]. In this case, the equilibrium pressure gradient force is linear in r, and the radial force-balance equation (29) reduces to the simple form given in Eq. (38). Equation (38) can be solved for the angular rotation velocity $\hat{\omega}_r$ to give

$$\hat{\omega}_r=\frac{\omega_c}{2}\pm\left[\left(\frac{\omega_c}{2}\right)^2+\omega_f^2-\frac{\hat{\omega}_p^2}{2}-\frac{2\hat{T}_\perp}{mr_b^2}\right]^{1/2}. \tag{94}$$

This result generalizes the previous cold-beam result in Eq. (75) to include finite thermal effects with $\hat{T}_\perp \neq 0$. The two solutions in Eq. (94) correspond to fast- and slow-rotational modes of the equilibrium. Beam launching conditions will determine the particular frequency selected. The condition for existence of a radially confined equilibrium that follows from Eq. (94) is $(\omega_c/2)^2+\omega_f^2 \geqslant \hat{\omega}_p^2/2+2\hat{T}_\perp/mr_b^2$. Contrasting this constraint with the cold-beam equilibrium constraint in Eq. (76), note that the addition of finite beam temperature ($\hat{T}_\perp \neq 0$) results in a lesser amount of space-charge ($\propto \hat{\omega}_p^2$) being confined for fixed values of ω_c and ω_f.

As indicated in Sec. IV, the step-function density profile assumed in the present analysis is a good approximation to those of more realistic beam distributions when the beam thermal emittance $\epsilon_{\rm th}$ is sufficiently small. However, the parabolic pressure profile $P_\perp^0(r)$ associated with the KV equilibrium may differ significantly from the pressure profiles characteristic of more realistic beam distributions. For example, in the limit of small thermal emittance, the density profile $n^0(r)$ of a thermal equilibrium beam is approximately uniform in the beam interior, and therefore the equilibrium pressure profile $P_\perp^0(r)=n^0T_\perp$, with $T_\perp=$const, is nearly constant in the beam interior, rather than parabolic. Such differences may significantly influence the fluid modes of the beam, particularly as the effects of finite temperature become appreciable. Nevertheless, because the transverse kinetic modes of a warm KV beam equilibrium are known analytically (see Appendix B), this simple case affords an ideal example that illustrates the consequences of the approximations inherent in the present warm-fluid model.

For the warm-fluid KV equilibrium, the eigenvalue equation (73) for axisymmetric flute perturbations can be simplified. Substituting Eqs. (34) and (35) into Eq. (73), the eigenvalue equation for the perturbed radial flow velocity δV_r can be expressed within the beam ($0 \leqslant r < r_b$) as

$$[\omega^2-\hat{\omega}_p^2-4(\hat{\omega}_r-\omega_c/2)^2]\delta V_r = -2\frac{\hat{T}_\perp}{m}\frac{\partial}{\partial r}\left[\frac{1}{r}\left(1-\frac{r^2}{r_b^2}\right)\frac{\partial}{\partial r}\,r\,\delta V_r\right]. \tag{95}$$

Motivated by analogy with Gluckstern's kinetic modes[11] for a warm KV beam (see Appendix B), we look for solutions to Eq. (95) where the perturbed potential $\delta\phi$ can be expanded within the beam in terms of a finite polynomial in r^2. Specifically, we take $\delta\phi=\delta\phi_n$, where

$$\delta\phi_n=\begin{cases}\displaystyle\sum_{j=0}^{n} a_j\left(\frac{r}{r_b}\right)^{2j}, & 0 \leqslant r < r_b,\\[2ex] \dfrac{\sum_{j=0}^{n} a_j}{\ln(r_w/r_b)}\ln\left(\dfrac{r_w}{r}\right), & r_b < r \leqslant r_w.\end{cases} \tag{96}$$

Here, n is a positive integer defining the cutoff of the power series expansion, and the a_j are expansion coefficients that must be determined consistent with the eigenvalue equation (95) and the boundary condition in Eq. (71). Note that the form of Eq. (96) satisfies the Poisson equation (66) outside the beam ($r_b < r \leqslant r_w$), is continuous at $r=r_b$, and vanishes at the conducting wall, i.e., $\delta\phi_n(r=r_w)=0$. It should also be pointed out, on general grounds, that one would expect that the expansion coefficients a_j to depend on the mode oscillation frequency ω as well as on equilibrium parameters.

Equation (69) can be applied to show that the perturbed radial flow velocity $\delta V_r=\delta V_{rn}$ corresponding to the potential expansion in Eq. (96) is given by

$$\delta V_{rn}=\frac{-2i\omega}{(4\pi q\hat{n})r_b}\sum_{j=1}^{n} j a_j\left(\frac{r}{r_b}\right)^{2j-1}, \tag{97}$$

within the beam. Substituting Eq. (97) into the eigenvalue equation (95), we obtain

$$\sum_{j=1}^{n-1}\left\{\left[\omega^2-\hat{\omega}_p^2-4(\hat{\omega}_r-\omega_c/2)^2-\frac{8\hat{T}_\perp}{mr_b^2}j^2\right]a_j + \frac{8\hat{T}_\perp}{mr_b^2}(j+1)^2 a_{j+1}\right\} j\left(\frac{r}{r_b}\right)^{2j-1} + a_n\left[\omega^2-\hat{\omega}_p^2-4(\hat{\omega}_r-\omega_c/2)^2-\frac{8\hat{T}_\perp}{mr_b^2}n^2\right] n\left(\frac{r}{r_b}\right)^{2n-1}=0. \tag{98}$$

The coefficients of each radial power in Eq. (98) must be set separately equal to zero for the expansions in Eqs. (96) and (97) to be valid. Therefore, the coefficient of the highest radial power, r^{2n-1}, yields the dispersion relation

$$\omega^2=\hat{\omega}_p^2+4(\hat{\omega}_r-\omega_c/2)^2+\frac{8\hat{T}_\perp}{mr_b^2}n^2. \tag{99}$$

Equation (99), together with setting the coefficients of successive powers of r^2 in the summation in Eq. (98) equal to zero yields the recursion relation

$$a_{j+1}=-\frac{n^2-j^2}{(j+1)^2}a_j \tag{100}$$

for $j=1,2,3,...,n-1$.

The jump condition at the beam edge radius r_b in Eq. (71) must also be satisfied. Substituting the perturbations in Eqs. (96) and (97) into Eq. (71) gives the requirement

$$\sum_{j=0}^{n}a_j=0. \tag{101}$$

Note from Eq. (96) that this condition implies that $\delta\phi_n=0$ at the beam edge ($r=r_b$) and in the vacuum region ($r_b<r\leqslant r_w$). Equation (101), together with the recursion relation (100) can be used to show that the eigenfunction expansion in Eq. (96) can be expressed succinctly as

$$\delta\phi_n=\begin{cases}\dfrac{A_n}{2}\left[P_{n-1}\left(1-2\dfrac{r^2}{r_b^2}\right)+P_n\left(1-2\dfrac{r^2}{r_b^2}\right)\right], & 0\leqslant r<r_b,\\ 0, & r_b<r\leqslant r_w.\end{cases} \tag{102}$$

Here, $P_n(x)$ denotes the nth-order Legendre polynomial, and $A_n=\text{const}$ denotes the linear mode amplitude, which can be identified in terms of the expansion coefficients a_j of the nth-order eigenmode expansion in Eq. (96) as $A_n=a_0$. Comparing Eqs. (96) and (102), we note that the expansion coefficients a_j are pure numbers, independent of both the equilibrium beam parameters and the mode oscillation frequency ω. Therefore, when expressed in terms of the normalized radial coordinate r/r_b, the radial mode structure is *independent* of both the equilibrium beam parameters and ω.

The radial eigenfunction (102) and the dispersion relation (99) specify the transverse fluid mode structure for perturbations about a warm KV beam equilibrium. Evidently, the dispersion relation (99) predicts stable oscillations with a single distinct value of ω^2 for all allowed equilibrium beam parameters. It should also be pointed out that stability is expected from general energy considerations applied to the warm-fluid KV beam equilibrium and certain other classes of rigidly rotating fluid equilibria.[55] For the important special cases of pure electric or pure magnetic focusing (see Appendix A) appropriate to model alternating gradient or solenoidal transport channels, respectively, the dispersion relation (99) can be expressed in alternative useful forms. For pure electric focusing with $\omega_c=0=\hat{\omega}_r$ and $\omega_f\neq 0$, the dispersion relation can be expressed as

$$\left(\frac{\omega}{\nu_0}\right)^2=2+2\left(\frac{\nu}{\nu_0}\right)^2(2n^2-1). \tag{103}$$

Here, $\nu^2\equiv\omega_f^2-\hat{\omega}_p^2/2=2\hat{T}_\perp/mr_b^2$ and $\nu_0^2\equiv\omega_f^2=2\hat{T}_\perp/mr_b^2+\hat{\omega}_p^2/2$ are the squares of the depressed and undepressed single-particle oscillation frequencies in the equilibrium field configuration [see Appendix A, Eqs. (A3) and (A4)]. The tune depression ν/ν_0 conveniently parametrizes the normalized mode oscillation frequency ω/ν_0 in Eq. (103). As shown in Appendix A, the limit $\nu/\nu_0\to 0$ corresponds to a cold, space-charge-dominated beam, and $\nu/\nu_0\to 1$, corresponds to a warm, temperature-dominated beam. On the other hand, for pure magnetic focusing with $\omega_f=0$ and $\omega_c\neq 0$, the dispersion relation (99) can be expressed conveniently as

$$\left(\frac{\omega}{\omega_c}\right)^2=\frac{\hat{\omega}_p^2}{\omega_c^2}+\left(1-\frac{2\hat{\omega}_p^2}{\omega_c^2}\right)n^2-\frac{4(\hat{\omega}_r-\omega_c/2)^2}{\omega_c^2}n^2. \tag{104}$$

Here, Eq. (94) has been used to eliminate $\hat{T}_\perp/mr_b^2$ in Eq. (99). Note that $(1-2\hat{\omega}_p^2/\omega_c^2)\geqslant 4(\hat{\omega}_r-\omega_c/2)^2/\omega_c^2$ is implied from the warm-beam equilibrium constraint equation (94) with $\hat{T}_\perp\geqslant 0$.

The mode structure is illustrated in Figs. 6 and 7. As a specific example, the electric focusing case is considered, and Eq. (103) is used in Fig. 6 to plot the normalized mode oscillation frequencies ω/ν_0 as a function of the tune depression ν/ν_0. Low-order solutions with radial mode numbers $n=1$ to $n=5$ are shown. Note that the cold-beam limit with $\nu/\nu_0\to 0$ and $\omega\to\pm\sqrt{2}\nu_0=\pm\hat{\omega}_p$ corresponds to the familiar long-wavelength ($k_z^2r_b^2\to 0$) limit found in Sec. IV A. The warm-beam limit with $\nu/\nu_0\to 1$ and $\omega\to\pm 2n\nu_0$ corresponds to collective oscillations in the absence of space-charge effects. In Fig. 7, the radial eigenfunctions corresponding to the modes of oscillation in Fig. 6 are plotted versus the normalized radial coordinate r/r_b. The radial mode structure is illustrated in terms of both the perturbed potential $\delta\phi_n(r)$ and the body-wave component of the perturbed density $\delta n_n(r)$ normalized to their on-axis values $\delta\phi_n(r=0)$ and $\delta n_n(r=0)$, respectively. Here, Eq. (102) is used to calculate the perturbed potential, and the corresponding perturbed density is determined in Eq. (C11) of Appendix C. Note that the radial mode structure is independent of the tune depression, ν/ν_0, and that the density perturbations become more peaked towards the beam edge ($r=r_b$) with increasing mode number n. The plots of the potential and density eigenfunctions in Fig. 7 are valid for all possible combinations of focusing fields (pure electric, pure magnetic, or combined electric and magnetic). The general structure of the eigenfunction in Eq. (102) is analyzed in detail in Appendix C. This analysis includes expansions of initial (time $t=0$) perturbations in density and potential in terms of the eigenfunctions $\delta\phi_n$, expressions for the eigenmode in terms of the perturbed density (δn) including singular surface-wave terms, and explicit power-series (in-r^2) expressions for the low-order eigenfunctions.

Gluckstern's kinetic treatment of transverse modes for perturbations about a KV beam equilibrium is reviewed in Appendix B for the case of pure electric focusing in the

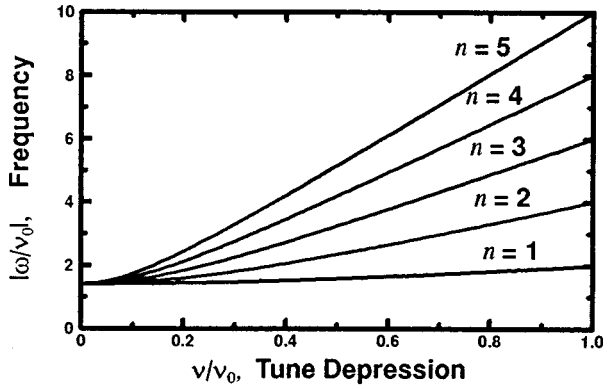

FIG. 6. Solutions for the normalized frequency $|\omega/\nu_0|$ of axisymmetric flute perturbations, calculated from the warm-fluid dispersion relation (103), are plotted as a function of the tune depression ν/ν_0 for a warm KV beam equilibrium with $\omega_c=0=\hat{\omega}_r$ and $\omega_f\neq 0$ in the electrostatic approximation. Frequencies are shown for radial mode numbers $n=1$, 2, 3, 4, and 5.

absence of beam rotation ($\omega_c=0=\hat{\omega}_r$ and $\omega_f\neq 0$). It is found that the radial eigenfunction obtained in the kinetic treatment [see Eq. (B9)] is *identical* to the expression derived in the present warm-fluid theory in Eq. (102) and Fig. 6. However, the dispersion relation derived in the kinetic theory [see Eq. (B10)] is strikingly different than the corresponding fluid dispersion relation in Eq. (103). To illustrate this, the oscillation frequencies supported by the fluid [Eq. (103)] and kinetic [Eq. (B10)] dispersion relations for a warm KV beam with pure electric focusing are contrasted in Fig. 8. Solutions of the nth-order polynomial (in ω^2) kinetic dispersion relation (solid curves) and the fluid dispersion relation (dashed curves) are plotted as a function of the tune depression ν/ν_0 for radial mode numbers $n=1,2,3,4$, and 5. The oscillation frequency Re ω and the growth rate Im ω are shown in absolute value because both $\pm\omega$ are solutions to the fluid and kinetic dispersion relations. For given radial mode number and tune depression, the fluid dispersion relation predicts stable oscillations with a single distinct value of ω^2, whereas the kinetic dispersion relation yields $2n$ possible modes of oscillation, some of which can become unstable (Im $\omega>0$) over a range of $\nu/\nu_0<0.3985$. The (identical) radial eigenmode structure of the fluid and kinetic modes illustrated in Fig. 7 is independent of both the tune depression, ν/ν_0, and the mode oscillation frequency, ω. Note that progressively more modes of oscillation become unstable in the kinetic model for higher radial mode number n. The kinetic mode structure illustrated in Figs. 7 and 8 is analyzed in greater detail in Appendix B. For present purposes, we note that the oscillation frequencies of the fluid modes closely track the (always stable) high-frequency kinetic branch with largest $|\omega|$ over the entire range of space-charge strength, $0\leqslant\nu/\nu_0\leqslant 1$. Moreover, the fluid and high-frequency kinetic oscillation frequencies become identical in the cold- and warm-beam limits, $\nu/\nu_0\to 0$ and $\nu/\nu_0\to 1$. For the special case of radial mode number $n=1$, the fluid and kinetic dispersion relations both reduce to the familiar envelope-mode dispersion relation,[2] $(\omega/\nu_0)^2=2+2(\nu/\nu_0)^2$, and the fluid and kinetic curves overlay exactly for $0\leqslant\nu/\nu_0\leqslant 1$ in Fig. 8(a).

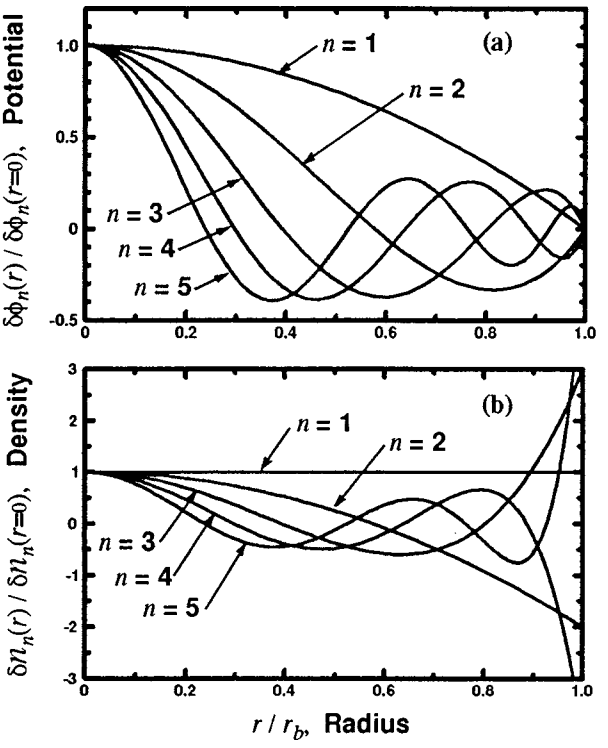

FIG. 7. Solutions for the normalized radial eigenfunction of axisymmetric flute perturbations are plotted as a function of normalized radial coordinate r/r_b for a warm KV beam equilibrium in the electrostatic approximation. The eigenfunction is plotted in terms of (a) the normalized potential $\delta\phi_n/\delta\phi_n(r=0)$, and (b) the normalized density $\delta n_n/\delta n_n(r=0)$, as calculated from Eqs. (102) and (C11), respectively, for radial mode numbers $n=1,2,...,$ and 5.

To interpret the mode comparisons in Fig. 8, we begin by pointing out that it is not surprising that the $n=1$ modes are identical in both the fluid and kinetic descriptions. It is expected on general grounds that the lowest-order perturbation about an equilibrium should reflect the structure of the equilibrium itself. In Appendix C, it is shown that the structure of the $n=1$ eigenfunction is equivalent to an infinitesimal change in equilibrium beam density with a corresponding, charge-conserving change in beam radius. Thus, this lowest-order perturbation reflects the structure of the equilibrium and corresponds to the situation encountered in an envelope model based on the assumption that the distribution evolution is self-similar to the equilibrium beam structure.[24] Furthermore, the moment equations derived in an envelope model are spatial averages of fluid equations. These considerations indicate that the exact $n=1$ mode agreement in Fig. 8(a) should be expected. Next, the lack of instability in the fluid description and the good agreement between the (stable) high-frequency kinetic and fluid modes can be qualitatively understood as follows. The present fluid model is based on the assumption of negligible heat flow, so it is not surprising that high-frequency oscillations are well-modeled for $\nu/\nu_0\ll 1$, because heat flow should be negligible for a cold beam on fast oscillation timescales. However, for the (stable) high-frequency branch, it is remarkable that the simple fluid dispersion relation approximates well the complicated, nth-order polynomial (in ω^2) kinetic dispersion re-

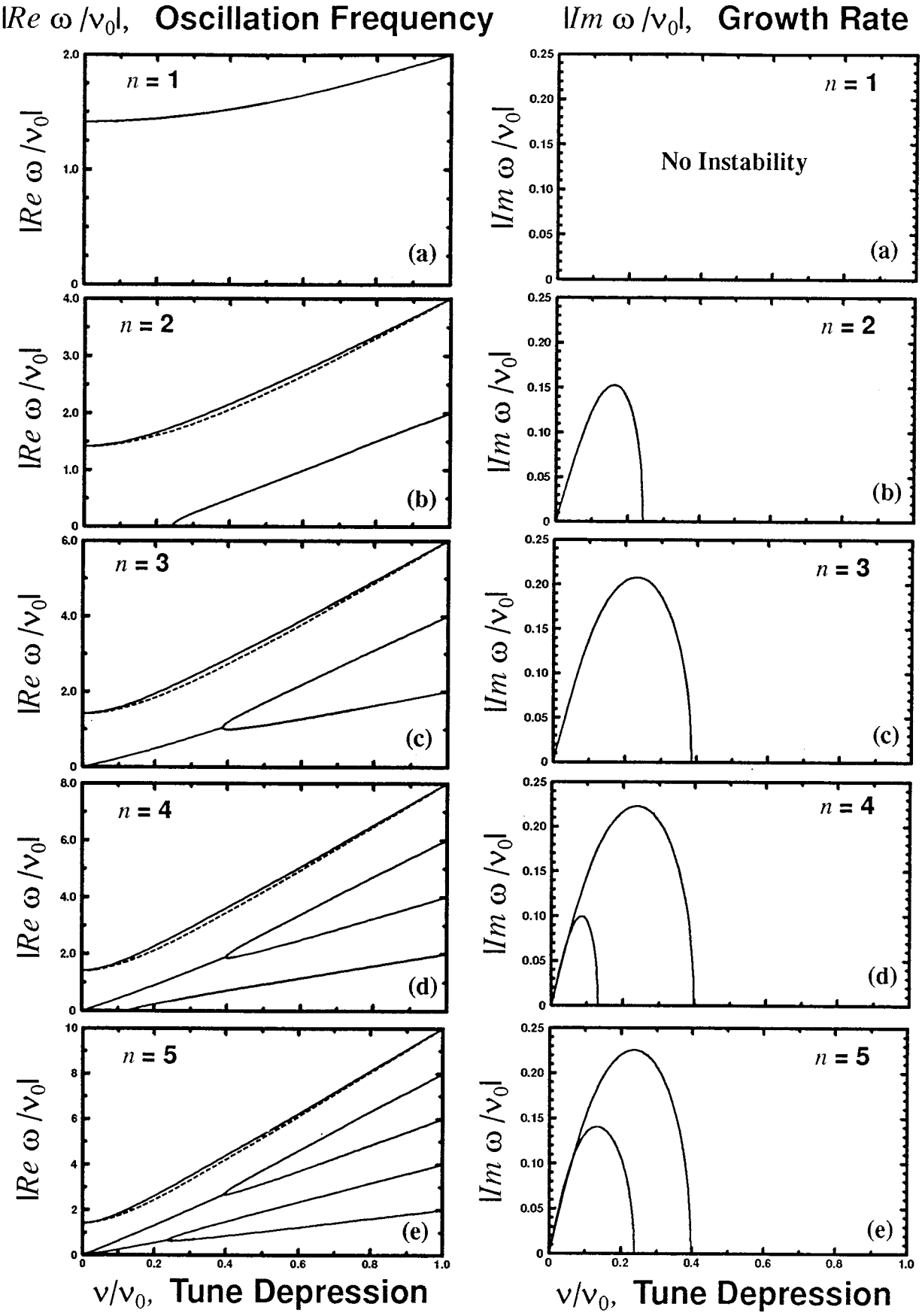

FIG. 8. Solutions for the normalized oscillation frequency $|\mathrm{Re}\ \omega/\nu_0|$ and growth rate $|\mathrm{Im}\ \omega/\nu_0|$ of axisymmetric flute perturbations, calculated from the kinetic dispersion relation (B10), are plotted (solid curves) as a function of the tune depression ν/ν_0 for a warm KV beam equilibrium with $\omega_c = 0 = \hat{\omega}_r$ and $\omega_f \neq 0$ in the electrostatic approximation. Results are shown for radial mode numbers $n = 1$, 2, 3, 4, and 5 in (a)–(e), and the normalized oscillation frequencies of the fluid modes shown in Fig. 6 are also plotted (dashed curves).

lation over the entire range of space-charge strength, $0 \leqslant \nu/\nu_0 \leqslant 1$, and becomes exact in the warm-beam limit $\nu/\nu_0 \to 1$. Evidently, for perturbations about a KV beam equilibrium, the neglected heat flow terms in Eq. (11) are negligible relative to the retained pressure terms for the highest-frequency mode. The lack of instability in the fluid model indicates that this approximation breaks down for lower-frequency modes, and the well-known kinetic instabilities for a KV beam indicated in Fig. 8 are not recovered. However, these kinetic instabilities are associated with the (unphysical) inverted phase-space population of the KV distribution (see Appendix B), and are not observed experimentally for more realistic phase-space distributions.[40,41] Thus, it may be preferable that the approximations inherent in the present warm-fluid model have removed such behavior. Note that kinetic beam distributions with monotonic decreasing phase-space populations are stable.[1] Such distributions are also necessarily stable in any fluid (moment) model and are not dissimilar in macroscopic properties to a KV beam equilibrium when $\nu/\nu_0 \ll 1$. From this perspective, it is not surprising that the present macroscopic model does not recover the instabilities inherent in a kinetic treatment of a KV beam.

The results presented here have a number of important implications. First, the analysis shows that certain, high-frequency kinetic modes supported by a KV beam equilibrium are well approximated by the present, warm-fluid model and are consequently a feature of the coarse, macroscopic structure of the equilibrium as opposed to the detailed phase-space structure. Such kinetic modes are *fluid-like*, whereas modes not obtained in the present fluid model are *kinetic-like* and require more details of the structure of the full distribution function. Because the macroscopic properties of the KV beam equilibrium are not too dissimilar from those of more physically realistic beams, these fluid-like modes are likely a good approximation to the high-frequency collective modes supported by beam equilibria with monotonically decreasing phase-space populations with $\partial F^0(H^0)/\partial H^0 \leqslant 0$ (see Appendix B). Such correspondences will, of course, be limited to time scales where kinetic effects such as Landau damping can be neglected. From this and other results presented here, we conclude that models based on an assumed, self-similar evolution of the beam distribution are of questionable validity for all but lowest-order (i.e., envelope-model) considerations. Even if a single, stable mode of oscillation is excited, the radial profiles of all macroscopic quantities would oscillate in time. Depending on measurement phases, no discernible perturbation may be observed at one phase, while later the perturbation reappears as the mode oscillates. Likely perturbations could, in practice, involve a spectrum of modes with differing oscillation frequencies. Poorly defined launching conditions can further complicate interpretations.[39] Higher-order structure resonances, etc., calculated under the assumption of self-similar distribution evolution could lead to erroneous conclusions. Finally, because the radial mode structure obtained in the kinetic and fluid models are identical, and the macroscopic properties of a KV beam equilibrium are similar to what is expected for a cold, space-charge-dominated beam, this suggests that the modes describing perturbations about a KV beam may form a reasonable basis state for characterizing perturbations in beam density—even for non-KV beams.

VI. CONCLUSIONS

A variety of modes of oscillation can be obtained from different theoretical models of charged-particle beams. Some models may predict instability in situations where others may not. It is important to analyze collective modes and instabilities using a hierarchy of model assumptions, so as to learn which features are model dependent and which have general applicability. In this paper, we have employed a warm-fluid model derived under the assumption of negligible heat flow and a diagonal pressure tensor to investigate the electrostatic stability properties of unbunched beams. Particular emphasis was placed on a KV beam equilibrium with uniform charge density and parabolic pressure profile. This was motivated by the fact that the kinetic modes that describe perturbations about a KV beam equilibrium are known analytically, affording an opportunity to better understand differences between the kinetic and fluid descriptions, and because the kinetic modes for a KV beam are frequently studied theoretically. The fluid modes were analyzed for perturbations about a KV equilibrium in both the cold-beam limit, and for axisymmetric transverse perturbations about a warm-beam equilibrium. The cold-beam results were used to examine the effects of finite beam canonical angular momentum on collective modes. The warm-fluid transverse stability results were compared with kinetic theory. It was shown that the fluid description reproduces exactly the radial eigenfunction obtained in kinetic theory but has a distinct (stable) oscillation frequency, in contrast to the multiplicity of (possibly unstable) frequencies obtained in the kinetic theory. This fluid-mode oscillation frequency approximates very well the highest-frequency kinetic mode, and is an important manifestation of the (physical) macroscopic features of the equilibrium, whereas the possibly unstable, lower-frequency kinetic modes depend on the (unphysical) inverted phase-space population of the equilibrium distribution. Implications of these results with regard to the interpretation of collective oscillations supported by realistic beam distributions were discussed. These results promise to increase our understanding of the evolution of density variations in intense beams—a topic of increasing importance in recent experiments.

It should be emphasized that the stability results presented in this paper were derived for beam focusing produced by the simultaneous presence of a continuous solenoidal magnetic field, $\mathbf{B}^{\rm sol} = B_f \hat{\mathbf{e}}_z$, and a continuous radial electric field, $\mathbf{E}^f = -(m/Z_i e)\omega_f^2 \mathbf{x}_\perp$. These fields represent that average focusing properties of a periodic lattice of solenoids, or a periodic lattice of alternating gradient quadrupoles (electric or magnetic), respectively. In practice, the stability results will typically be applied for pure magnetic focusing ($\mathbf{E}^f = 0$ and $\mathbf{B}^{\rm sol} \neq 0$) and a rigidly rotating beam equilibrium ($\hat{\omega}_r \neq 0$), or for pure electric focusing ($\mathbf{E}^f \neq 0$ and $\mathbf{B}^{\rm sol} = 0$) and a nonrotating beam equilibrium ($\hat{\omega}_r = 0$). Also, as explained in Sec. IV, in the pure magnetic focusing case the beam is typically launched with zero canonical an-

gular momentum in order to achieve a minimum beam radius, corresponding to equilibrium beam rotation at the Larmor frequency, $\hat{\omega}_r = Z_i e B_f/2mc = \omega_c/2$. In this case, it is shown in Appendix A that the pure magnetic and the pure electric focusing cases are equivalent under the correspondence $\omega_f^2 \Leftrightarrow (\omega_c/2)^2$. Here, we have retained both electric and magnetic focusing components explicitly to allow analysis of beam stability with nonzero canonical angular momentum ($\hat{\omega}_r \neq \omega_c/2$), and to allow easy identification of appropriate substitutions to analyze other focusing cases not directly considered.

Finally, for simplicity of presentation, the stability analysis presented here has been carried out for the case of a *nonrelativistic* ion beam. It should be emphasized, however, that the warm-fluid formalism is readily extended to the case of an intense ion beam propagating in the axial direction with relativistic average axial velocity V_b and relativistic mass factor $\gamma_b = (1 - V_b^2/c^2)^{-1/2}$, provided the ion motion in the *beam frame* (''primed'' coordinates) is nonrelativistic with ion velocities satisfying $|\mathbf{v}'| \ll c$, and the directed axial velocity V_b is large relative to particle velocities in the beam frame, i.e., $V_b \gg |\mathbf{v}'|$. These restrictions are met in the regimes of practical interest for heavy-ion fusion and the intense proton accelerators envisioned for tritium production and spallation neutron sources. For completeness, the relativistic generalizations of the cold- and warm-beam stability analyses in Secs. IV and V, consistent with the inequalities $|\mathbf{v}'| \ll c$ and $V_b \gg |\mathbf{v}'|$, are presented in Appendix D.

ACKNOWLEDGMENTS

The authors wish to thank John Barnard, Irving Haber, Ingo Hofmann, and Tai-Sen Wang for useful discussions.

This research was performed under the auspices of the U.S. Department of Energy at the Lawrence Livermore National Laboratory under Contract No. W-7405-ENG-48, and at the Princeton Plasma Physics Laboratory under Contract No. DE-ACOZ-76-CHO-3073, and in part by the Office of Naval Research.

APPENDIX A: PARTICLE ORBITS IN A KV BEAM EQUILIBRIUM

In this appendix, we analyze the transverse dynamics of particles in the equilibrium field configuration of a KV beam to better understand the implications of changing equilibrium parameters on the particle motion. Using the notation employed in Sec. III A, we examine the motion of a particle with transverse coordinate $\mathbf{x}_\perp$ moving within the beam ($0 \leqslant r < r_b$). The equation of motion of the particle is given by

$$\frac{d^2}{dt^2}\mathbf{x}_\perp = -\left(\omega_f^2 - \frac{\hat{\omega}_p^2}{2}\right)\mathbf{x}_\perp + \omega_c \frac{d}{dt}\mathbf{x}_\perp \times \hat{\mathbf{e}}_z . \tag{A1}$$

Denoting $Z = x + iy$, the equation of motion (A1) can be expressed as $d^2Z/dt^2 = -(\omega_f^2 - \hat{\omega}_p^2/2)Z + i\omega_c dZ/dt$. The solution to this equation can be expressed as $Z = \hat{Z}\exp(-i\nu t)$, where $\hat{Z}$ is a complex amplitude determined from the initial conditions of the particle motion, and $\nu = \text{const}$ is the particle oscillation frequency. Substituting this expression into the equation of motion gives $\nu^2 + \omega_c \nu - (\omega_f^2 - \hat{\omega}_p^2/2) = 0$, or equivalently,

$$\nu = -\frac{\omega_c}{2} \pm \frac{1}{2}(\omega_c^2 + 4\omega_f^2 - 2\hat{\omega}_p^2)^{1/2}. \tag{A2}$$

All particles in a KV beam equilibrium undergo transverse oscillations in the presence of the applied focusing field and the defocusing space-charge field at the frequencies defined in Eq. (A2). The two solutions for ν correspond to fast and slow modes of particle oscillation in the equilibrium field, and are symmetrically located above and below the Larmor frequency, $-\omega_c/2$.

In most practical applications of the present model, the beam will be subject to pure electric focusing ($\omega_c = 0$, and $\omega_f \neq 0$) and will not be in a state of macroscopic rotation ($\hat{\omega}_r = 0$), or will be subject to pure magnetic focusing ($\omega_f = 0$ and $\omega_c \neq 0$) and will be in a state of macroscopic rotation ($\hat{\omega}_r \neq 0$). These two cases model the average focusing properties of a periodic lattice of alternating-gradient quadrupoles (electric or magnetic), or a periodic lattice of solenoids, respectively. We now analyze, in turn, both of these special cases in greater detail.

In the pure electric focusing case with $\omega_c = 0 = \hat{\omega}_r$ and $\omega_f \neq 0$, the square of the single-particle oscillation frequency in Eq. (A2) reduces to

$$\nu^2 = \omega_f^2 - \frac{\hat{\omega}_p^2}{2} = \frac{2\hat{T}_\perp}{mr_b^2}. \tag{A3}$$

Here, we have employed the equilibrium constraint condition, $\omega_f^2 = \hat{\omega}_p^2/2 + 2\hat{T}_\perp/mr_b^2$, which follows from Eq. (94) with $\omega_c = 0 = \hat{\omega}_r$. The orbital oscillation frequency ν in Eq. (A3) is commonly referred to as the *depressed* betatron frequency. It is also convenient to define an *undepressed* betatron frequency

$$\nu_0^2 = \omega_f^2 = \frac{2\hat{T}_\perp}{mr_b^2} + \frac{\hat{\omega}_p^2}{2}, \tag{A4}$$

by taking $\nu \to \nu_0$ and $\hat{\omega}_p^2 \to 0$ in Eq. (A3). Note from Eqs. (A3) and (A4) that ν_0 corresponds to the oscillation frequency of a single particle in the applied focusing field which is proportional to ω_f^2, and that $\nu^2 = \nu_0^2 - \hat{\omega}_p^2/2$, showing that the actual particle oscillation frequency in the presence of space-charge ($\hat{\omega}_p^2 \neq 0$) is *depressed* from the applied-field value. The ratio ν/ν_0 is referred to as the *tune depression* and provides a convenient, dimensionless measure of space-charge strength in the equilibrium beam, with $\nu/\nu_0 \to 0$ corresponding to a cold, space-charge-dominated beam with $\hat{T}_\perp \to 0$ and $\hat{\omega}_p^2/2 \to \omega_f^2$, and $\nu/\nu_0 \to 1$ corresponding to a temperature-dominated beam with $\hat{T}_\perp/m\hat{\omega}_p^2 r_b^2 \to \infty$. The fact that Eq. (A4) predicts a single, distinct particle oscillation frequency $|\nu|$ follows from the absence of an applied magnetic field ($\omega_c = 0$) and macroscopic beam rotation ($\hat{\omega}_r = 0$).

In the pure magnetic focusing case with $\omega_f = 0$, $\omega_c \neq 0$, and $\hat{\omega}_r \neq 0$, it is convenient to rewrite Eq. (A2) in the Larmor frame, rotating about the beam axis ($r = 0$) with angular ve-

locity $-\omega_c/2$. In the Larmor frame, the frequency of transverse particle oscillations is $\nu' = \nu + \omega_c/2$. Equation (A2) then reduces to

$$(\nu')^2 = \left(\frac{\omega_c}{2}\right)^2 - \frac{\hat{\omega}_p^2}{2} = \frac{2\hat{T}_\perp}{mr_b^2} + (\hat{\omega}_r - \hat{\omega}_c/2)^2. \tag{A5}$$

Here, we have employed the equilibrium constraint condition $(\hat{\omega}_r - \omega_c/2)^2 = (\omega_c/2)^2 - \hat{\omega}_p^2/2 - 2\hat{T}_\perp/mr_b^2$, which follows from Eq. (94) with $\omega_f = 0$. As expected, Eq. (A5) has the same form as Eq. (A3) with the focusing term ω_f^2 replaced by $(\omega_c/2)^2$ and $\hat{T}_\perp$ replaced by $\hat{T}_\perp + m(\hat{\omega}_r - \hat{\omega}_c/2)^2 r_b^2/2$. This ''shifted'' measure of temperature includes contributions from both the thermal emittance $\epsilon_{\rm th}^2 = 2\hat{T}_\perp r_b^2/mV_b^2$ [Eq. (41)] and the directed emittance $\epsilon_d^2 = (2\langle P_\theta\rangle/mV_b^2)^2$ [Eq. (41)] appropriate for a beam with canonical angular momentum $\langle P_\theta\rangle = -m(\hat{\omega}_r - \omega_c/2)r_b^2/2$ [Eq. (40)]. Note that the directed emittance ϵ_d vanishes for a beam with zero canonical angular momentum rotating at the Larmor frequency ($\hat{\omega}_r = \omega_c/2$).

The correspondence between the pure electric and pure magnetic focusing cases discussed above can be understood more generally in terms of a simple transformation argument. Assuming a general distribution of beam space-charge (not necessarily a KV equilibrium), it is clear from the Vlasov–Poisson system in Eqs. (5)–(7) that the equations of motion of a particle with transverse coordinate $\mathbf{x}_\perp$ and axial coordinate z are

$$\frac{d^2}{dt^2}\,\mathbf{x}_\perp = -\omega_f^2\mathbf{x}_\perp + \omega_c\,\frac{d}{dt}\,\mathbf{x}_\perp \times \hat{\mathbf{e}}_z - \frac{Z_i e}{m}\,\nabla_\perp\phi, \tag{A6}$$

$$\frac{d^2}{dt^2}\,z = -\frac{Z_i e}{m}\,\frac{\partial\phi}{\partial z}, \tag{A7}$$

where ϕ is the electrostatic potential for the average self-electric field. To transform the transverse equations of motion to the Larmor frame (''primed'' coordinates) rotating with angular velocity $-\omega_c/2$ about the $\hat{\mathbf{e}}_z$ axis, we define

$$\begin{aligned} x' &= x\,\cos\frac{\omega_c}{2}\,t - y\,\sin\frac{\omega_c}{2}\,t, \\ y' &= x\,\sin\frac{\omega_c}{2}\,t + y\,\cos\frac{\omega_c}{2}\,t. \end{aligned} \tag{A8}$$

In the Larmor frame, Eq. (A6) is expressed as

$$\frac{d^2}{dt^2}\,\mathbf{x}_\perp' = -\left[\omega_f^2 + \left(\frac{\omega_c}{2}\right)^2\right]\mathbf{x}_\perp' - \frac{Z_i e}{m}\,\nabla_\perp'\phi. \tag{A9}$$

Note that the equation of motion (A6) in the laboratory frame for pure electric focusing ($\omega_c = 0$) is identical to the equation of motion (A9) in the Larmor frame for pure magnetic focusing ($\omega_f = 0$) provided we make the replacement $(\omega_c/2)^2 \to \omega_f^2$. Therefore, if the radial profiles for the pure electric-focused and magnetic-focused equilibria are identical, and the magnetic-focused equilibrium is rigidly rotating with angular velocity $\hat{\omega}_r = \omega_c/2$ [see the equilibrium force balance equation (29) and note the rotation sense defined in Eq. (28)] so that the equilibrium is ''nonrotating'' in the Larmor frame, it follows that the Larmor-frame stability analysis of the magnetic-focused equilibrium will be identical (in primed variables) to the stability analysis of the electric-focused equilibrium under the correspondence $(\omega_c/2)^2 \Leftrightarrow \omega_f^2$. In this context, a rigidly rotating, magnetic-focused beam equilibrium with zero canonical angular momentum ($\hat{\omega}_r = \omega_c/2$) can be regarded as equivalent to a nonrotating beam equilibrium with pure electric focusing. This result holds for both the fluid and kinetic descriptions.

APPENDIX B: TRANSVERSE KINETIC MODES OF A KV BEAM

In this appendix, we summarize results from a kinetic stability analysis of a continuously focused, warm KV beam equilibrium. Gluckstern[11–13] and other authors[14–19] have employed an electrostatic Vlasov–Poisson model to derive analytically the normal-mode structure of transverse ($k_z = 0$) flute perturbations about a KV beam equilibrium. We refer to these modes as *Gluckstern modes*. For present purposes, the summary here is limited to the case of symmetric perturbations ($\partial/\partial\theta = 0$) with azimuthal mode number $l = 0$.

For simplicity, we consider a nonrotating ($\hat{\omega}_r = 0$) beam with pure electric focusing ($B_f = 0$ and $\omega_f^2 \neq 0$). The Vlasov–Poisson equations (5)–(7) for the transverse ($\partial/\partial z = 0$) distribution function $F(\mathbf{x}_\perp, \mathbf{p}_\perp, t) = \int dp_z\, f(\mathbf{x}_\perp, \mathbf{p}, t)$ can be expressed as

$$\begin{aligned} &\left\{\frac{\partial}{\partial t} + \frac{\partial H}{\partial \mathbf{p}_\perp}\cdot\frac{\partial}{\partial \mathbf{x}_\perp} - \frac{\partial H}{\partial \mathbf{x}_\perp}\cdot\frac{\partial}{\partial \mathbf{p}_\perp}\right\}F(\mathbf{x}_\perp, \mathbf{p}_\perp, t) = 0, \\ &\nabla_\perp^2\phi = -4\pi Z_i e\int dp_x dp_y\, F, \\ &\phi(r = r_w, \theta, t) = \text{const.} \end{aligned} \tag{B1}$$

Here,

$$H = \frac{\mathbf{p}_\perp^2}{2m} + m\,\frac{\nu_0^2}{2}\,\mathbf{x}_\perp^2 + Z_i e\,\phi(\mathbf{x}_\perp, t) \tag{B2}$$

is the single-particle Hamiltonian, and $\nu_0 = \omega_f$ denotes the frequency of undepressed particle oscillations in the applied focusing field [see Appendix A, Eq. (A4)]. Perturbations with $\partial/\partial\theta = 0$ are assumed and expanded according to

$$\begin{aligned} \phi &= \phi^0(r) + \delta\phi(r, \omega)\exp(-i\omega t), \\ F &= F^0(\mathbf{x}_\perp, \mathbf{p}_\perp) + \delta F(r, \mathbf{p}_\perp, \omega)\exp(-i\omega t), \end{aligned} \tag{B3}$$

where equilibrium quantities (superscript zero) correspond to $\partial/\partial t = 0$ solutions to Eqs. (B1) and (B2) with $\delta\phi = 0 = \delta F$. For present purposes, we assume a KV equilibrium distribution defined by[1,2]

$$F^0(\mathbf{x}_\perp, \mathbf{p}_\perp) = \frac{\hat{n}}{2\pi m}\,\delta(H^0 - \hat{T}_\perp). \tag{B4}$$

Here, $\delta(x)$ is the Dirac delta function, $\hat{n} = \text{const}$, and $\hat{T}_\perp = \text{const}$. Note that all particles in the distribution function F^0 have the same value of single-particle energy in the equilibrium fields ($H^0 = \hat{T}_\perp$), constituting a highly inverted population in phase space where the entire distribution will participate in any instability. It follows trivially from the Hamiltonian form of the Vlasov equation (B1) that the KV distribution F^0 specified by Eq. (B4) [or any other function $F^0(H^0)$] is a valid equilibrium solution ($\partial/\partial t = 0$) when $\delta\phi = 0 = \delta F$. The form of F^0 in Eq. (B4) is consistent with a

uniform beam density, $\int dp_x dp_y\, F^0 = \hat{n}$, and a parabolic pressure profile, $\int dp_x dp_y\, (\mathbf{p}_\perp^2/2m) F^0 = \hat{n}\hat{T}_\perp (1 - r^2/r_b^2)$, in the beam interior ($0 \leq r < r_b$). Here,

$$r_b^2 = \frac{2\hat{T}_\perp/m}{\nu_0^2 - \hat{\omega}_p^2/2} \tag{B5}$$

is the square of the equilibrium beam radius, $\hat{\omega}_p^2 = 4\pi Z_i^2 e^2 \hat{n}/m$ is the plasma frequency squared, and the constraint equation (B5) is identical to the envelope equation given in Eq. (38) with $\hat{\omega}_r = 0 = \omega_c$, or in Eq. (42) with $\epsilon_d = 0 = \omega_c$.

The linear eigenvalue equation for the perturbed potential $\delta\phi(r,\omega)$ can be derived as follows. First the perturbations (B3) are substituted into the Vlasov–Poisson equations (B1), and the equations are expanded to linear order in $\delta\phi$ and δF. Then the *linearized* Vlasov equation is solved for δf using the method of characteristics.[1] This solution can then be substituted into the linearized Poisson equation to obtain the eigenvalue equation

$$\frac{1}{r}\frac{\partial}{\partial r} r \frac{\partial}{\partial r}\, \delta\phi = \hat{\omega}_p^2 \Theta(r_b - r) \times \left[\frac{1}{v_\perp}\frac{\partial}{\partial v_\perp} I_{\rm orb}\right]\Bigg|_{v_\perp^2 = (2\hat{T}_\perp/m)(1 - r^2/r_b^2)} + \frac{\hat{\omega}_p^2 r_b}{2\hat{T}_\perp/m}\, \delta(r - r_b)[\delta\phi + I_{\rm orb}]\big|_{v_\perp = 0}. \tag{B6}$$

Here, $v_\perp = p_\perp/m$, $\Theta(x)$ is the Heaviside step function defined by $\Theta(x) = 1$ for $x > 0$ and $\Theta(x) = 0$ for $x < 0$, and

$$I_{\rm orb}(r, v_\perp, \omega) = i\omega \int_{-\pi}^{\pi} \frac{d\psi}{2\pi} \int_{-\infty}^{0} d\tau\, \delta\phi[\tilde{r}(\tau), \omega] \times \exp(-i\omega\tau) \tag{B7}$$

is the orbit integral.[1,11] In Eqs. (B6) and (B7), Im $\omega > 0$ is assumed (corresponding to instability), and

$$\tilde{r}^2(\tau) = r^2 \cos^2(\nu\tau) + \frac{r v_\perp}{\nu}\cos(\psi)\sin(2\nu\tau) + \frac{v_\perp^2}{\nu^2}\sin^2(\nu\tau) \tag{B8}$$

is the radial trajectory of a particle in the equilibrium field configuration, with ''initial'' conditions ($\tau = 0$) corresponding to $\tilde{x}(0) = r\cos\theta$, $\tilde{y}(0) = r\sin\theta$, $\tilde{p}_x(0) = p_\perp \cos\phi_p$, and $\tilde{p}_y(0) = p_\perp \sin\phi_p$. Here, $\psi \equiv \theta - \phi_p$, and $\nu = (\nu_0^2 - \hat{\omega}_p^2/2)^{1/2} = (2\hat{T}_\perp/m r_b^2)^{1/2}$ denotes the frequency of transverse particle oscillations in the full (applied- plus self-) field configuration of the KV beam equilibrium [see Appendix A, Eq. (A3)]. The terms on the right-hand side of the eigenvalue equation (B6) multiplying the step and delta functions represent body- and surface-wave perturbations, respectively.

It can be shown[11,15] that the integro-differential equation (B6) subject to the boundary condition $\delta\phi(r = r_w) = 0$ supports normal-mode solutions, $\delta\phi = \delta\phi_n$, that can be expanded as a finite polynomial in r^2 as

$$\delta\phi_n = \begin{cases} \dfrac{A_n}{2}\left[P_{n-1}\left(1 - 2\dfrac{r^2}{r_b^2}\right) + P_n\left(1 - 2\dfrac{r^2}{r_b^2}\right)\right], & 0 \leq r < r_b, \\ 0, & r_b < r \leq r_w. \end{cases} \tag{B9}$$

Here, $n = 1,2,3,...$ is the radial mode number, $A_n = $ const is the linear amplitude parameter of the mode, and $P_n(x)$ is the nth-order Legendre polynomial. Each n-labeled eigenfunction, $\delta\phi_n$, has $2n$ distinct frequencies ω satisfying an nth-degree polynomial (in ω^2) dispersion relation that can be expressed in normalized form as

$$2n + \frac{1 - (\nu/\nu_0)^2}{(\nu/\nu_0)^2}\left[B_{n-1}\left(\frac{\omega/\nu_0}{\nu/\nu_0}\right) - B_n\left(\frac{\omega/\nu_0}{\nu/\nu_0}\right)\right] = 0. \tag{B10}$$

Here, $B_n(\alpha)$ is defined by

$$B_n(\alpha) \equiv \begin{cases} 1, & n = 0, \\ \dfrac{[(\alpha/2)^2 - 0^2]}{[(\alpha/2)^2 - 1^2]}\dfrac{[(\alpha/2)^2 - 2^2]}{[(\alpha/2)^2 - 3^2]} \cdots \dfrac{[(\alpha/2)^2 - (n-1)^2]}{[(\alpha/2)^2 - n^2]}, & n = 1,3,5,..., \\ \dfrac{[(\alpha/2)^2 - 1^2]}{[(\alpha/2)^2 - 2^2]}\dfrac{[(\alpha/2)^2 - 3^2]}{[(\alpha/2)^2 - 4^2]} \cdots \dfrac{[(\alpha/2)^2 - (n-1)^2]}{[(\alpha/2)^2 - n^2]}, & n = 2,4,6,... . \end{cases} \tag{B11}$$

This explicit polynomial form of the dispersion relation was first derived by Wang and Smith.[15] Note that the normalized mode frequency ω/ν_0 depends on the single dimensionless equilibrium parameter, ν/ν_0, the tune depression of the beam. Explicit polynomial representations of the kinetic dispersion relation are summarized in Table I for radial mode numbers $n = 1$ to $n = 5$ in terms of the dimensionless variables $\overline{\omega} \equiv \omega/\nu_0$ and $\overline{\nu} \equiv \nu/\nu_0$.

The structure of the eigenfunction (B9) for the Gluckstern modes is analyzed in detail in Appendix C. Plots of low-order eigenfunctions are presented in Fig. 7, both in terms of the perturbed potential ($\delta\phi$) and the perturbed density ($\delta n = \int dp_x dp_y\, \delta F$) for $0 \leq r < r_b$. Plots of low-order solutions to the dispersion relation (B10) are presented in Fig. 8. Because $\pm\omega$ are both solutions to the polynomial (in ω^2) dispersion relation, only the absolute values of the real

TABLE I. Kinetic dispersion relation calculated from Eq. (B10) for electrostatic perturbations with radial mode numbers $n=1$ to $n=5$ about a warm *KV* beam equilibrium. Here, $\bar{\omega}=\omega/\nu_0$ and $\bar{\nu}=\nu/\nu_0$.

Mode n	Dispersion relation
1	$\bar{\omega}^2-2(1+\bar{\nu}^2)=0$
2	$\bar{\omega}^4-2(1+9\bar{\nu}^2)\bar{\omega}^2-4\bar{\nu}^2(1-17\bar{\nu}^2)=0$
3	$\bar{\omega}^6-2(1+27\bar{\nu}^2)\bar{\omega}^4+8(1+97\bar{\nu}^2)\bar{\nu}^2\bar{\omega}^2-96(1+23\bar{\nu}^2)\bar{\nu}^4=0$
4	$\bar{\omega}^8-2(1+59\bar{\nu}^2)\bar{\omega}^6+52(1+83\bar{\nu}^2)\bar{\nu}^2\bar{\omega}^4-32(19+1621\bar{\nu}^2)\bar{\nu}^4\bar{\omega}^2-288(9-521\bar{\nu}^2)\bar{\nu}^6=0$
5	$\bar{\omega}^{10}-2(1+109\bar{\nu}^2)\bar{\omega}^8+48(3+338\bar{\nu}^2)\bar{\nu}^2\bar{\omega}^6-64(57+7588\bar{\nu}^2)\bar{\nu}^4\bar{\omega}^4+128(97+42055\bar{\nu}^2)\bar{\nu}^6\bar{\omega}^2-23040(9+631\bar{\nu}^2)\bar{\nu}^8=0$

and imaginary parts of ω are plotted. Note from Eq. (B9) and Fig. 7 that the radial structure of the nth-order eigenfunction is independent of the values of the $2n$ solutions for ω supported by the dispersion relation. As evident from Fig. 8, all branches are stable ($\mathrm{Im}\,\omega=0$) in the warm-beam limit with $\nu/\nu_0\to 1$, and have oscillation frequency $\omega/\nu_0=\pm 2,\pm 4,...,\pm 2n$. In the cold-beam limit with $\nu/\nu_0\to 0$, there are two stable solutions with $\omega=\pm\sqrt{2}\nu_0=\pm\hat{\omega}_p$, and all other solutions are marginally stable with $\omega\to 0$. For general tune depressions, $0\leqslant\nu/\nu_0\leqslant 1$, the lowest-order solution with $n=1$ describes the well-known linear envelope mode corresponding to stable oscillations in the beam radius r_b at frequency $\omega=\pm\nu_0[2+2(\nu/\nu_0)^2]^{1/2}$.[2] Unstable solutions with $\mathrm{Im}\,\omega>0$ can exist for mode numbers $n>1$. For a given value of n, the high-frequency branch with the largest $|\omega|$ is always stable for $0\leqslant\nu/\nu_0\leqslant 1$. Unstable branches with smaller values of $|\omega|$ exist for ν/ν_0 less than the threshold values of ν/ν_0 where two stable branches with real ω intersect. The growth rates of these unstable branches achieve a maximum at some value of ν/ν_0 below the threshold value for onset of instability, before decreasing to zero (i.e., $\mathrm{Im}\,\omega\to 0$) in the cold-beam limit with $\nu/\nu_0\to 0$. The branch with maximum instability threshold first becomes unstable at $\nu/\nu_0=0.2425$, 0.3859, 0.3985, and 0.3972 for mode numbers $n=2$, 3, 4, and 5, respectively. This instability threshold is maximum for $n=4$ and slowly decreases with increasing n for $n>4$. Generally, for increasing mode number n, more branches of ω are found to be unstable at low values of ν/ν_0. Such high-order instabilities are a consequence of the highly inverted (singular) population of the KV equilibrium distribution F^0, and will not occur for equilibrium distributions $F^0(H^0)$ that are monotonically decreasing functions of H^0 with $\partial F^0/\partial H^0\leqslant 0$, which are known to be stable.[1]

Finally, it should be noted that the stability results derived in this appendix for the case of a nonrotating KV beam equilibrium with pure electric focusing can be applied to a KV beam equilibrium with zero canonical angular momentum and pure magnetic focusing using the transformation arguments presented in Appendix A.

APPENDIX C: STRUCTURE OF THE EIGENFUNCTIONS FOR GLUCKSTERN MODES

In this appendix, we analyze properties of the Gluckstern-mode eigenfunctions for azimuthally symmetric ($l=0$), electrostatic flute perturbations ($k_z=0$) about a warm KV beam equilibrium with edge radius r_b. Specifically, the structure of the eigenfunctions, when expressed in terms of the perturbed potential ($\delta\phi$) and the perturbed density (δn), is examined. Because the eigenfunctions are the same in these variables for both the warm-fluid [see Sec. V, Eq. (102)] and kinetic [see Appendix B, Eq. (B9)] theories presented in this manuscript, all results presented here apply to both models.

First, we demonstrate that the Gluckstern modes can be used to describe an arbitrary perturbation in density or potential. Let $\delta n(r)$ represent an initial (time $t=0$) perturbation in density about a warm KV beam equilibrium. Other than having small amplitude ($|\delta n|/\hat{n}\ll 1$), the radial structure of the perturbation is arbitrary. The Poisson equation (66) can be solved subject to the boundary condition $\delta\phi(r=r_w)=0$ at the conducting wall in order to express the initial density perturbation $\delta n(r)$ in terms of the corresponding perturbation in electrostatic potential $\delta\phi(r)$. We introduce the scaled radial coordinate

$$X=1-2\left(\frac{r}{r_b}\right)^2. \tag{C1}$$

For values of radius r extending from the beam center to the beam edge, $0\leqslant r\leqslant r_b$, note that $-1\leqslant X\leqslant 1$, where $X=1$ and $X=-1$ correspond to the beam center ($r=0$) and edge ($r=r_b$), respectively. In terms of X, the Poisson equation (66) can be expressed conveniently as

$$\pi Z_i e r_b^2\delta n(X)=2\frac{\partial}{\partial X}\left[\frac{(X^2-1)}{X+1}\frac{\partial}{\partial X}\,\delta\phi(X)\right]. \tag{C2}$$

Because the Legendre polynomials $P_n(X)$ form a complete, orthogonal set on the interval $-1\leqslant X\leqslant 1$, it follows that $\delta\phi$ can be expanded within the beam as

$$\delta\phi(X)=\sum_{n=0}^{\infty} C_n P_n(X), \tag{C3}$$

where the constants C_n are given by

$$C_n=\frac{2n+1}{2}\int_{-1}^{1} dX\; P_n(X)\,\delta\phi(X). \tag{C4}$$

The expansion (C3) can be expressed in the equivalent form

$$\delta\phi(X)=\sum_{n=1}^{\infty}\delta\phi_n(X), \tag{C5}$$

where

$$\delta\phi_n(X)=\frac{A_n}{2}\left[P_{n-1}(X)+P_n(X)\right] \tag{C6}$$

are the Gluckstern eigenfunctions describing normal-mode perturbations within the warm-fluid [see Eq. (102)] or kinetic [see Eq. (B9)] models, as expressed in terms of $X=1-2r^2/r_b^2$, and the coefficients A_n and C_n are related by

$$A_n=2\sum_{j=0}^{n-1}(-1)^{n+1+j}C_j. \tag{C7}$$

TABLE II. Normalized body-wave ($0 \leqslant r < r_b$) eigenfunctions for the potential ($\delta\phi_n$) and density (δn_n) for electrostatic perturbations with radial mode numbers $n=1$ to $n=5$ about a warm *KV* beam equilibrium. Here, $\bar{r} = r/r_b$, and the perturbations in potential and density are calculated from Eqs. (C6) and (C11), respectively. The results apply to both the warm-fluid and kinetic models.

Mode n	Potential $\delta\phi_n/A_n$	Density $\pi Z_i e r_b^2 \delta n_n / A_n$
1	$1-\bar{r}^2$	1
2	$1-4\bar{r}^2+3\bar{r}^4$	$4(1-3\bar{r}^2)$
3	$1-9\bar{r}^2+18\bar{r}^4-10\bar{r}^6$	$9(1-8\bar{r}^2+10\bar{r}^4)$
4	$1-16\bar{r}^2+60\bar{r}^4-80\bar{r}^6+35\bar{r}^8$	$16(1-15\bar{r}^2+45\bar{r}^4-35\bar{r}^6)$
5	$1-25\bar{r}^2+150\bar{r}^4-350\bar{r}^6+350\bar{r}^8-126\bar{r}^{10}$	$25(1-24\bar{r}^2+126\bar{r}^4-224\bar{r}^6+126\bar{r}^8)$

In Eq. (C5), we have implicitly enforced continuity of $\delta\phi_n$ at the edge radius r_b of the beam. The inverse of the transformation specified by Eq. (C7) is

$$C_0 = A_1/2, \qquad C_n = \frac{A_n + A_{n+1}}{2}, \quad j = 1,2,3,\ldots . \tag{C8}$$

These results explicitly demonstrate for a warm KV beam equilibrium that an arbitrary initial perturbation in density $[\delta n(r)]$ or potential $[\delta\phi(r)]$ can be expanded in terms of the eigenfunctions $\delta\phi_n(r)$. This analysis does not address the general completeness problem, which requires showing that arbitrary initial pressure and flow velocity perturbations can be simultaneously represented in the present fluid model. Such considerations are important in understanding the launching conditions for collective waves.

We now investigate the radial structure of the nth-order Gluckstern eigenfunction $\delta\phi_n$. As evident from Eq. (C6), the eigenfunction $\delta\phi_n$ is expressed simply within the beam as a sum two Legendre polynomials, P_{n-1} and P_n, with argument $X = 1 - 2r^2/r_b^2$. It is useful to note that at the beam center ($r=0$ and $X=1$) and the beam edge ($r=r_b$ and $X=-1$), the results $P_n(1)=1$ and $P_n(-1)=(-1)^n$ show that the eigenfunction $\delta\phi_n$ has values

$$\delta\phi_n(r=0) = A_n, \qquad \delta\phi_n(r=r_b) = 0. \tag{C9}$$

Because $\delta\phi_n = 0$ at the beam edge, $r=r_b$, it follows from the Poisson equation (66) that $\delta\phi_n$ must vanish outside the beam ($r_b < r \leqslant r_w$). The vanishing of $\delta\phi_n$ in the vacuum region is consistent with Eqs. (102) and (B9). For reference, the eigenfunctions $\delta\phi_n$ are presented in explicit, expanded form in Table II for radial mode numbers $n=1$ to $n=5$. These expressions are valid over the range $0 \leqslant r \leqslant r_b$, and are presented in terms of the scaled radial coordinate $\bar{r} \equiv r/r_b$. In general, the nth-order eigenfunction $\delta\phi_n$ has n nodes ($\delta\phi_n = 0$) and n antinodes ($\delta\phi_n$ at relative maxima or minima with $\partial\delta\phi_n/\partial r = 0$) over the range $0 \leqslant r \leqslant r_b$. The tabulated eigenfunctions $\delta\phi_n$ are plotted in Fig. 7(a).

Finally, for completeness, we express the Gluckstern eigenfunction defined in Eq. (C6) in terms of the perturbed density (δn) rather than the perturbed potential ($\delta\phi$). Using the Poisson equation (66) with $\delta\phi = \delta\phi_n$ and $\delta n = \delta n_n$ along with the corresponding perturbed fluid (Sec. III D) or kinetic equations (Appendix B), it can be shown that the density representation of the Gluckstern eigenfunction, δn_n, can be expressed as

$$\delta n_n = \delta n_n(r)|_{\text{body}} \Theta(r_b - r) + \delta n_n|_{\text{surface}} \frac{r_b^2}{r} \delta(r - r_b). \tag{C10}$$

Here, $\Theta(x)$ is the Heaviside step function defined by $\Theta(x) = 1$ for $x > 0$ and $\Theta(x) = 0$ for $x < 0$, and $\delta(x)$ is the Dirac delta function. The step and delta functions in Eq. (C10) multiply the ''body-wave'' and ''surface-wave'' terms, $\delta n_n|_{\text{body}}$ and $\delta n_n|_{\text{surface}}$, which specify the smooth density perturbation within the beam ($0 \leqslant r \leqslant r_b$) and the singular density perturbation at the beam edge ($r = r_b$), respectively. The body-wave component, $\delta n_n|_{\text{body}}$, can be calculated in terms of the scaled radial coordinate $X = 1 - 2(r/r_b)^2$ from the Poisson equation (C2) and recursion relations for the Legendre polynomials. We obtain

$$\begin{aligned}\pi Z_i e r_b^2 \delta n_n|_{\text{body}} &= \frac{A_n}{(X^2-1)(X+1)} \{(n-1)(n-2)P_{n-3}(X) \\ &+ (n-1)[(n-1) - 2X(n-2)]P_{n-2}(X) \\ &+ [(2n-1)(X-1) - n(n-1)X - n^2 X \\ &+ (n-1)^2 X^2]P_{n-1}(X) + [n(X-1) + n^2X^2]P_n(X)\}.\end{aligned} \tag{C11}$$

The amplitude of the surface-wave component, $\delta n_n|_{\text{surface}}$, can be calculated using the fact that the perturbation introduces zero net charge into the system, or equivalently, that $\int_0^{r_w} dr\, r\, \delta n_n = 0$. This implies that $r_b^2 \delta n_n|_{\text{surface}} = -\int_0^{r_b(1-\epsilon)} dr\, r\, \delta n_n|_{\text{body}}$, where $\epsilon \to 0^+$. This integral can be carried out using the Poisson equation (66) and recursion relations for the Legendre polynomials to show that

$$\pi Z_i e r_b^2 \delta n_n|_{\text{surface}} = (-1)^n \frac{nA_n}{2}. \tag{C12}$$

The singular surface-charge perturbation given by Eqs. (C10) and (C12) is the manifestation, within linear theory, of a perturbation induced by a small change in beam radius, δr_b, with $|\delta r_b|/r_b \ll 1$. To understand this, note that the total (equilibrium plus perturbed) density can be expressed as $n(r) = [\hat{n} + \delta n_n(r)|_{\text{body}}]\Theta(r_b - r) + \delta n_n|_{\text{surface}}(r_b^2/r)\delta(r$

$-r_b)$, where $n^0(r)=\hat{n}\Theta(r_b-r)$ is the equilibrium density profile defined in Eq. (34), and r_b is the equilibrium beam radius. To linear order, this equation can be expressed equivalently as

$$n(r)=[\hat{n}+\delta n_n(r)|_{\rm body}]\Theta\left[r_b+(-1)^n\frac{nA_n}{2\pi Z_i e\hat{n}r_b}-r\right]$$
$$=[\hat{n}+\delta n_n(r)|_{\rm body}]\Theta[r_b+\delta r_b-r], \tag{C13}$$

which shows that the surface-wave perturbation can be interpreted as a change in beam radius, $\delta r_b=(-1)^n(nA_n/2\pi Z_i e\hat{n}r_b)$. Aside from the complication of the mode description associated with this surface term, it is evident from the form of the body-wave density perturbation in Eq. (C11) and the form of the corresponding potential perturbation in Eq. (C6) that the Gluckstern eigenfunction is expressed more simply in terms of $\delta\phi_n$ than in terms of δn_n. Nevertheless, Eqs. (C10)–(C12) can be useful to interpret the mode structure in practical situations because the profile of the beam charge density is often directly measured experimentally. At the beam center ($r=0$ and $X=1$) and the beam edge [$r=r_b(1-\epsilon)$ and $X=-1+4\epsilon$ where $\epsilon\to 0^+$], it can be shown that the nonsingular, body-wave component of the density eigenfunction δn_n given by Eq. (C11) has the values

$$\pi Z_i e r_b^2\delta n_n(r=0)|_{\rm body}=n^2A_n,$$
$$\pi Z_i e r_b^2\delta n_n(r=r_b)|_{\rm body}=(-1)^{n+1}n^3A_n. \tag{C14}$$

In contrast to the potential eigenfunction $\delta\phi_n$, which vanishes as r approaches the beam edge [$r=r_b(1-\epsilon)$ with $\epsilon\to 0^+$], the density eigenfunction $\delta n_n|_{\rm body}$ is nonzero and becomes large with increasing mode index n. For reference, explicit representations of the body-wave component of the eigenfunction δn_n are presented in Table II for radial mode numbers $n=1$ to $n=5$. The presentation format is analogous to that used to represent the eigenfunction $\delta\phi_n$ in Table II. For the nth-order eigenfunction, δn_n, it is found that there are $n-1$ nodes ($\delta n_n=0$) and $n-1$ antinodes (δn_n at relative maxima or minima with $\partial\delta n_n/\partial r=0$) within the beam ($0\leqslant r<r_b$). The tabulated eigenfunctions δn_n are plotted in Fig. 7(b).

APPENDIX D: RELATIVISTIC GENERALIZATIONS

We consider an ion beam propagating in the z direction with average axial velocity V_b and relativistic mass factor $\gamma_b=(1-\beta_b^2)^{-1/2}$, where $\beta_b=V_b/c$. In situations where the ion motion in the beam frame (''primed'' coordinates) is nonrelativistic with $|\mathbf{v}'|\ll c$, and the velocity of directed ion motion is large relative to ion velocities in the beam frame with $V_b\gg|\mathbf{v}'|$, the nonrelativistic electrostatic formalism developed in Secs. II–V is readily extended to the relativistic regime. This can be carried out through the use of the Lorentz transformations appropriate for the electrostatic potential, $\phi'=\gamma_b(\phi-\beta_bA_z)$, the z component of the vector potential, $A_z'=\gamma_b(A_z-\beta_b\phi)$, and the wave frequency and axial wave number, $\omega'=\gamma_b(\omega-k_zV_b)$ and $k_z'=\gamma_b(k_z-\omega\beta_b/c)$. Particularly important, for nonrelativistic motion in the beam frame, is the fact that $A_z'\simeq 0$, which gives $A_z=\beta_b\phi$ and $\phi-\beta_bA_z=(1-\beta_b^2)\phi=\phi/\gamma_b^2$.

We present here, without giving a detailed derivation, the relativistic generalizations of the cold-beam and warm-beam fluid stability results in Secs. IV and V, valid for $|\mathbf{v}'|\ll c$ and $V_b\gg|\mathbf{v}'|$. Common to both analyses is the equilibrium force balance equation (38), which is generalized in the relativistic case to become

$$\hat{\omega}_r(\omega_c/\gamma_b-\hat{\omega}_r)+\omega_f^2/\gamma_b-\frac{2\hat{T}_\perp/\gamma_b m}{r_b^2}$$
$$=\frac{2Z_i^2e^2N_b}{\gamma_b^3mr_b^2}=\frac{\hat{\omega}_p^2}{2\gamma_b^3}. \tag{D1}$$

Here, $\gamma_b=(1-\beta_b^2)^{-1/2}$ is the relativistic mass factor, and $\hat{\omega}_p^2=4\pi\hat{n}Z_i^2e^2/m$ and $\omega_c=Z_ieB_f/mc$ are the nonrelativistic plasma frequency-squared and the cyclotron frequency, respectively.

First we consider the cold-beam ($\hat{T}_\perp\to 0$) stability results of Sec. IV, derived for the step-function density profile in Eq. (79) and general values of azimuthal harmonic number l and axial wave number k_z. The relativistic generalization of the full cold-beam dispersion relation in Eq. (83) is given by

$$k_zr_b\frac{K_l(k_zr_w)I_l'(k_zr_b)-K_l'(k_zr_b)I_l(k_zr_w)}{K_l(k_zr_w)I_l(k_zr_b)-K_l(k_zr_b)I_l(k_zr_w)}$$
$$-\left[1-\frac{\hat{\omega}_p^2/\gamma_b}{\Omega^2-4(\hat{\omega}_r-\omega_c/2\gamma_b)^2}\right]Tr_b\frac{J_l'(Tr_b)}{J_l(Tr_b)}$$
$$=-2l\frac{(\hat{\omega}_p^2/\gamma_b)(\hat{\omega}_r-\omega_c/2\gamma_b)}{\Omega[\Omega^2-4(\hat{\omega}_r-\omega_c/2\gamma_b)^2]}. \tag{D2}$$

Here, identical to the nonrelativistic case, Ω is defined by $\Omega=\omega-l\hat{\omega}_r-k_zV_b$, while the coefficient T occurring in Eq. (D2) is relativistically generalized as

$$T^2=-k_z^2\frac{1-\hat{\omega}_p^2/\gamma_b^3\Omega^2}{1-\hat{\omega}_p^2/\gamma_b[\Omega^2-4(\hat{\omega}_r-\omega_c/2\gamma_b)^2]}. \tag{D3}$$

The relativistic generalization of the eigenfunction in Eq. (80) is identical in form provided Eq. (D3) is used in place of Eq. (81) to define T^2. Moreover, the equilibrium parameters $\hat{\omega}_p^2$, ω_c, $\hat{\omega}_r$, and γ_b occurring in Eqs. (D2) and (D3) are related by the generalized equilibrium force balance condition (D1) with $\hat{T}_\perp=0$. Other results presented in Sec. IV can be generalized to the relativistic case in the obvious manner.

Next we consider the stability results of Sec. V, derived for the case of a warm KV beam equilibrium with axisymmetric flute perturbations ($l=0$ and $k_z=0$). The dispersion relation (99) is generalized to become

$$\omega^2=\hat{\omega}_p^2/\gamma_b+4(\hat{\omega}_r-\omega_c/2\gamma_b)^2+\frac{8\hat{T}_\perp}{\gamma_b mr_b^2}n^2, \tag{D4}$$

and the eigenfunction given by Eq. (102) is unchanged in form. Again, the equilibrium parameters are related by Eq. (D1), and other results presented in Sec. V can be generalized in the obvious manner.

Finally, it should be pointed out that the two differing relativistic factors occurring in the terms involving the plasma frequency-squared in Eqs. (D1)–(D4), $\hat{\omega}_p^2/\gamma_b$ and $\hat{\omega}_p^2/\gamma_b^3$, correspond to corrections due to leading-order kinematic effects and combined kinematic/magnetic self-field effects, respectively. Also, similar arguments to those presented here can be used to obtain the relativistic generalizations of the kinetic stability analysis summarized in Appendix B.

[1] R. C. Davidson, *Physics of Nonneutral Plasmas* (Addison–Wesley, Reading, MA, 1990), and references therein.
[2] M. Reiser, *Theory and Design of Charged Particle Beams* (Wiley, New York, 1994).
[3] H. Wiedemann, *Particle Accelerator Physics* (Springer, New York, 1993), Vols. I and II.
[4] J. D. Lawson, *The Physics of Charged-Particle Beams* (Oxford Science, New York, 1988).
[5] E. P. Lee and J. Hovingh, Fusion Technol. **15**, 369 (1989).
[6] R. A. Jameson, in *Advanced Accelerator Concepts*, Port Jefferson, NY, 1992, edited by J. S. Wurtele [AIP Conf. Proc. **279**, 969 (1993)].
[7] R. W. Muller, in *Nuclear Fusion by Inertial Confinement: A Comprehensive Treatise*, edited by G. Velarde, Y. Ronen and J. M. Martinez-Val (CRC, Boca Raton, FL, 1993), Chap. 17, pp. 437–453.
[8] See, for example, *Proceedings of the 1995 International Symposium on Heavy Ion Inertial Fusion*, edited by J. J. Barnard, T. J. Fessenden and E. P. Lee [J. Fusion Eng. Design **32**, 1-620 (1996)], and references therein.
[9] A. Friedman, R. O. Bangerter, and W. B. Hermannsfeldt, in *Proceedings of the IAEA Technical Committee Meeting on Drivers for Inertial Confinement Fusion, Paris, France, 1994* (Commisariat a l'Energie Atomique, Saclay, France, 1995), p. 243.
[10] I. Kapchinskij and V. Vladimirskij, in *Proceedings of the International Conference on High Energy Accelerators and Instrumentation* (CERN Scientific Information Service, Geneva, 1959), p. 274.
[11] R. L. Gluckstern, in *Proceedings of the 1970 Proton Linear Accelerator Conference, Batavia, IL, 1971*, edited by M. R. Tracy (National Accelerator Laboratory, Batavia, IL, 1971), p. 811.
[12] R. L. Gluckstern, W.-H. Cheng, and H. Yee, Phys. Rev. Lett. **75**, 2835 (1995).
[13] R. L. Gluckstern, W.-H. Cheng, S. S. Kurennoy, and H. Ye, Phys. Rev. E **54**, 6788 (1996).
[14] T.-S. Wang and L. Smith, IEEE Trans. Nucl. Sci. **NS-28**, 2399 (1981).
[15] T.-S. Wang and L. Smith, Part. Accel. **12**, 247 (1982).
[16] H. S. Uhm and R. C. Davidson, Phys. Fluids **23**, 1586 (1980).
[17] H. S. Uhm and R. C. Davidson, Part. Accel. **11**, 65 (1980).
[18] I. Hofmann, L. J. Laslett, L. Smith, and I. Haber, Part. Accel. **13**, 145 (1983).
[19] I. Hofmann, ''Stability of anisotropic beams with space charge,'' Phys. Rev. E (in press).
[20] G. P. Saraph and M. Reiser, Part. Accel. **49**, 15 (1995).
[21] C. Chen, R. Pakter, and R. C. Davidson, Phys. Rev. Lett. **79**, 225 (1997).
[22] C. Chen and R. C. Davidson, Phys. Rev. Lett. **72**, 2195 (1994).
[23] C. Chen and R. C. Davidson, Phys. Rev. E **49**, 5679 (1994).
[24] E. P. Lee and R. K. Cooper, Part. Accel. **7**, 83 (1976).
[25] I. Hofmann, Adv. Electron. Electron Phys. Suppl. **13C**, 49 (1983).
[26] I. Hofmann and J. Struckmeier, Part. Accel. **21**, 69 (1987).
[27] M. Reiser, J. Appl. Phys. **70**, 1919 (1991).
[28] J. Struckmeier and I. Hofmann, Part. Accel. **39**, 219 (1992).
[29] R. C. Davidson and S. M. Lund, in *Thomas H. Stix Symposium on Advances in Plasma Physics*, Princeton, NJ, 1992, edited by N. J. Fisch [AIP Conf. Proc. **314**, 1 (1994)].
[30] N. Brown and M. Reiser, Phys. Plasmas **2**, 965 (1995).
[31] R. C. Davidson and C. Chen, ''Kinetic description of intense nonneutral beam propagation through a periodic solenoidal focusing field based on the nonlinear Vlasov–Maxwell equations,'' Part. Accel. (in press).
[32] R. C. Davidson, W. W. Lee, and P. Stoltz, Phys. Plasmas **5**, 279 (1998).
[33] J. Struckmeier and J. Klabunde, Part. Accel. **15**, 47 (1984).
[34] A. Friedman and D. P. Grote, Phys. Fluids B **4**, 2203 (1992).
[35] I. Haber, D. A. Callahan, A. Friedman, D. P. Grote, and A. B. Langdon, J. Fusion Eng. Design **32**, 159 (1996).
[36] I. Haber, D. A. Callahan, A. Friedman, D. P. Grote, S. M. Lund, and T.-F. Wang, ''Transverse-longitudinal temperature equilibration in a bounded nonneutral plasma,'' Nucl. Instrum. Methods Phys. Res. (in press).
[37] W. W. Lee, Q. Qian, and R. C. Davidson, Phys. Lett. A **230**, 347 (1997).
[38] Q. Qian, W. W. Lee, and R. C. Davidson, Phys. Plasmas **4**, 1915 (1997).
[39] S. M. Lund, J. J. Barnard, G. D. Craig, A. Friedman, D. P. Grote, H. S. Hopkins, T. C. Sangster, W. M. Sharp, S. Eylon, T. J. Fessenden, E. Henestroza, S. Yu, and I. Haber, ''Numerical simulation of intense-beam experiments at LLNL and LBNL,'' Nucl. Instrum. Methods Phys. Res. (in press).
[40] M. G. Tiefenback, ''Space-Charge Limits on the Transport of Ion Beams in a Long Alternating Gradient System, Ph.D. thesis, University of California, Berkeley, 1986 (Lawrence Berkeley Laboratory Publication, LBL-22465, 1986).
[41] W. M. Fawley, T. Garvey, S. Eylon, E. Henestroza, A. Faltens, T. J. Fessenden, K. Hahn, L. Smith, and D. P. Grote, Phys. Plasmas **4**, 880 (1997).
[42] S. Yu, S. Eylon, E. Henestroza, and D. Grote, in *Space Charge Dominated Beams and Applications of High Brightness Beams*, Bloomington, IN, 1995, edited by S. Y. Lee [AIP Conf. Proc. **377**, 134 (1996)].
[43] S. S. Yu, S. Eylon, E. Henestroza, C. Peters, L. Reginato, A. Tauschwitz, D. Grote, and F. Deadrick, J. Fus. Eng. Design **32**, 309 (1996).
[44] M. Reiser, C. R. Chang, D. Kehne, K. Low, T. Shea, H. Rudd, and I. Haber, Phys. Rev. Lett. **61**, 2933 (1988).
[45] F. J. Sacherer, IEEE Trans. Nucl. Sci. **NS-18**, 1105 (1971).
[46] See, e.g., Chaps. 2, 4, 9 and 10 of Ref. 1.
[47] Reference 1 presents a general derivation of the macroscopic fluid-Maxwell equations from the Vlasov–Maxwell equations on pages 22–26. Several aspects of cold-fluid equilibrium and stability properties of nonneutral beam-plasma systems are described on pages 240–276 of Ref. 1.
[48] R. C. Davidson, *Handbook of Plasma Physics-Basic Plasma Physics*, edited by M. N. Rosenbluth and R. Z. Sagdeev (North-Holland, Amsterdam, 1984), Vol. 2, pp. 729–819.
[49] I. Hofmann, IEEE Trans. Nucl. Sci. **NS-26**, 3083 (1979).
[50] G. A. Krafft, J. W.-K. Mark, and T.-S. Wang, SIAM (Soc. Ind. Appl. Math.) J. Appl. Math. **43**, 1390 (1983).
[51] R. C. Davidson, B. H. Hui, and C. A. Kapetanakos, Phys. Fluids **18**, 1040 (1975).
[52] R. C. Davidson and B. H. Hui, Ann. Phys. (N.Y.) **94**, 209 (1975).
[53] M. Reiser, Phys. Fluids **20**, 477 (1977).
[54] R. C. Davidson, P. Stoltz, and C. Chen, Phys. Plasmas **4**, 3710 (1997).

[55] The authors wish to thank Ed Lee for bringing to our attention energy arguments analogous to those employed in magnetohydrodynamics [see, for example, G. Schmidt, *Physics of High Temperature Plasmas* (Academic, New York, 1979)] can be used in the present warm-fluid model to bound perturbations for rigidly-rotating fluid equilibria with radial profiles satisfying certain derivative conditions. This can be used to show that the macroscopic profiles for a KV beam equilibrium satisfy a sufficient condition for fluid stability.